Petrographic and X-Ray Diffraction Analyses of Samples from Coso Geothermal Wells 33A-7, 33A-7 St-1 and 83-11

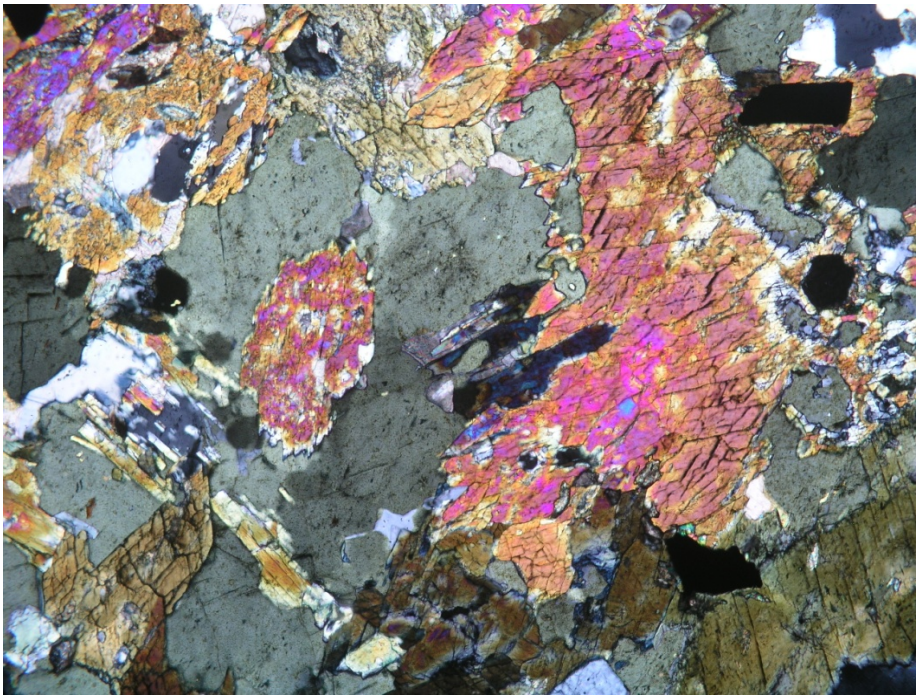

Prepared for:
Coso Operating Company, LLC
P.O. Box 1690
Inyokern CA 93527-1690

By:
Clay Jones and Joseph Moore
Energy & Geoscience Institute
Salt Lake City, Utah
February 7, 2011

1.0 INTRODUCTION

At the request of Mr. J. McCulloch, cuttings samples Coso wells 33A-7, 33A-7 ST-1 and 83-11 were studied to determine the distribution of rock types encountered in the wells, the effects of hydrothermal alteration, and the processes that led to mineral deposition. Petrographic and X-ray diffraction (XRD) analyses were performed on 84 samples. These analyses were conducted on samples ranging in depth from 6960 to 8300 ft in 33A-7, from 8100 to 10160 ft in 33A-7ST-1 and from 6780 to 8310 in 83-11. The study focused primarily on the lower portions of the wells where permeability and high temperatures were encountered. Comparison of the wells indicates that samples from 33A-7 and 33A-7 ST-1 are similar. However there are interesting differences in the rock types and veins encountered in these wells and those studied in 83-11.

2.0 ROCK TYPES

The cuttings samples studied include diorite, granite, rhyolite, and traces of amphibolite. Representative photomicrographs of each cuttings sample are shown in Appendix A (33A-7), B (33A-7 ST-1) and C (83-11); key textural and mineralogical relationships are shown in the figures accompanying the text. The distribution of rock types in the three wells is shown in figure 2.1.

Diorite is the dominant rock type in all three wells. It is common throughout 83-11 and in the upper portions of the sampled intervals in the 33A-7 wells. Samples from these three wells are typical of the diorite found in other parts of the field. They are characterized by intergrown plagioclase, amphibole, biotite, epidote and titanite (figs. 2.2 to 2.7; mineral descriptions in captions refer to the upper image in each figure). Although the diorites display textures characteristic of intrusive rocks the mineral assemblages are diagnostic of the greenschist facies of regional metamorphism. Deformation related to metamorphism is commonly represented by kinked plagioclase crystals (fig. 2.7).

A few percent quartz and primary potassium feldspar may be present in some samples of diorite, (refer to table 3.1), which is a common feature throughout the field. These rocks are more appropriately classified as quartz diorite. However, secondary potassium feldspar (adularia[1]) is common and there is abundant petrographic evidence in the samples studied for the replacement of plagioclase by adularia (figs. 2.2 and 2.6; also 3.18 and 3.18). Compositionally, rocks logged as diorite span a range of rock types from diorite to quartz diorite, granodiorite and quartz monzodiorite based on the relative abundances of plagioclase, potassium feldspar, and quartz. These rocks are difficult to distinguishing in cuttings samples because of the effects of hydrothermal alteration.

Alteration is variable, ranging from weak to intense. Examples are shown in the appendices and following figures. Adularia, illite, calcite and epidote replace plagioclase and chlorite replaces hornblende and biotite.

[1] The term adularia refers to a geothermal potassium feldspar. It typically occurs as rhombic crystals in veins and as a replacement of plagioclase feldspar.

The diorites are typically more extensively altered, brecciated and veined than other rock types found at Coso, although the alteration minerals are similar. These relationships have been interpreted to indicate the diorites are older than the granodiorite, granite and rhyolite (see Moore and others, 2004).

Amphibolites are relatively uncommon at Coso. They consist of varying proportions of amphiboles, and in places biotite and epidote. They are metamorphic rocks, but their origin is not well understood. Some may represent high temperature veins, others metasediments. Amphibolite consisting of actinolite, biotite and epidote was encountered in 33A-7 ST-1 at a depth of 7120 ft (fig. 2.8). We attach no particular geothermal significance to their presence.

Granite occurs sporadically in 83-11 and is common in the lower portion of the 33A-7 wells (fig. 2.9 to 2.13). In 33A-7 ST-1, granite is present within a 200 ft interval between 7780 and 7880 ft. The limited distribution of the granite is interpreted to indicate it forms dikes within the diorite. Granite is readily identified in the cuttings samples by its light color and weak alteration. It is commonly fine-grained and porphyritic, consisting of nearly equal amounts of plagioclase, potassium feldspar and quartz and minor biotite. Granophyric textures (intergrowths of quartz and potassium feldspar) are widespread and serve to distinguish the granite from other rock types. Similar intergrowth textures were observed in 46A-19 RD. Rarely, traces red garnet are present (fig. 2.13). Alteration of the granite is generally weak and reflected in the presence of minor illite and epidote after plagioclase and chlorite after biotite. The weak alteration compared to the diorite and granodiorite found in other wells suggests that the granite is theyoungest of the major intrusive rocks within the geothermal reservoir.

Few age dates are available on rocks from the Coso geothermal field. One of these dates was obtained by Moore and others (2004) on potassium feldspar from a garnet-bearing granite from a depth of 4700.1 ft in well 58-10. The thermal history of the granite was determined by $^{40}Ar/^{39}Ar$ spectrum dating performed at the New Mexico Geochronological Research Laboratory by Dr. M. Heizler. The technique uses a step-heating process to release Ar incrementally, thus producing data from which thermal histories can be modeled via the Multiple Diffusion Domain (MDD) method (Lovera et al., 1989). This method models potassium-feldspar crystals as containing discrete diffusion domains of varying size. All the domains have the same diffusivity and activation energy, but the smaller diffusion domains release Ar more readily and at a lower temperature than the larger domains, because there is a shorter distance for the Ar to travel. The domains are considered to be separated by physical boundaries within the crystals. These boundaries may be cleavage planes, twinning lamellae, fractures, perthite lamellae or grain boundaries.

When potassium feldspar is naturally heated, Ar is lost from the crystal. The degree of Ar loss is dependent on the temperature the crystal is subjected to, the length of time it is exposed to that temperature and the crystal's domain structure. The shape of the measured age spectrum will therefore be a function of its thermal history. The spectrum can then be modeled using various time-temperature histories. A good match between the measured and modeled age spectra of this sample was achieved if the sample is cooled quickly from ~350^{o}C at 53 Ma to ~150^{o}C by ~50 Ma followed by cooling to ~100^{o}C by 30 Ma. The age of 53 Ma was interpreted as representing

the age of emplacement. It was also concluded that the granite has not been heated above its present temperature since 30 Ma.

Rhyolite was encountered in the 33A-7 wells. It appears to be a major dike forming rock between 9100 and 9500 ft in 33A-7 ST-1. Elsewhere in the field, rhyolite is uncommon. We suggest these rhyolite dikes represent the conduits that produced the rhyolite domes on the west flank of the field. Sugarloaf has been dated at 360,000 years and it is likely that some of the other domes on the west flank are contemporaneous. Irrespective of the absolute age of the rhyolite, it can be inferred that the alteration assemblages they contain are part of the recent geothermal history of Coso. These assemblages and their significance are discussed below.

The rhyolite is characterized by spherulitic devitrification textures and intergrowths of potassium feldspar and quartz (figs. 2.14 to 2.17). X-ray analyses of the rhyolite (e.g. 9160 to 9300 ft in 33A7-ST-1) show nearly equal concentrations of plagioclase and potassium feldspar and slightly lower concentrations of quartz. Minor hornblende and biotite in this interval is interpreted to represent contamination by chips of diorite.

The rhyolite is locally silicified (figs. 2.16 and 2.17). Rarely traces of epidote as vug fillings and veins are present.

3.0 HYDROTHERMAL ALTERATION

The distribution and origin of the hydrothermal minerals was determined using a combination of XRD analyses and thin section petrography. X-ray diffraction analyses are essential for evaluating clay mineral distributions. Smectite and interlayered illite-smectite, in particular, have a significant influence on the geophysical signatures of geothermal systems because of their electrical conductivities. The distributions of these clay minerals are particularly sensitive to variations in temperature. The thin sections provide information on mineral textures and relative age relationships.

X-Ray Diffraction Methodology

Whole-rock and clay X-ray diffraction XRD analyses were preformed on each sample in the XRD laboratory at the Energy & Geoscience Institute at the University of Utah, using a Bruker D8 Advance X-ray diffactometer. Phase quantification using the Reitveld method was performed using TOPAS software, developed by Bruker Analytical X-ray Systems. The principal of the Reitveld method is that the intensities calculated from a model of the crystalline structure are fit to the observed X-ray powder pattern by a least squares refinement. This is done by varying the parameters of the crystal structures and of the peak profiles to minimize the difference between observed and calculated powder patterns. Because the whole powder pattern is taken into consideration, problems of peak overlap are minimized and accurate quantitative analyses can be obtained.

The following operating parameters were used when analyzing the powdered samples: Cu-K-α radiation at 40 kV and 40 mA, $0.02^{o}2\theta$ step size, and 0.4 and 0.6 seconds per step for clay and bulk samples respectively. Clay samples were examined from 2 to $45^{o}2\theta$, and the bulk sample

from 4 to 65^{o}2θ. The instrument is equipped with a detector (lynx eye) that collects data over 2.6 mm, rather than at a point, greatly increasing X-ray counts collected, and decreasing acquisition time; a rotating sample stage which increases the mineral grain orientations encountered by the incident electron beam; and an automated sample exchanger capable of holding up to 45 samples.

Three analyses were conducted on each sample after being ground in a micronizing mill until fine enough to pass through a 325 mesh screen (particle size < 44 micrometers). The crushed sample was split into two fractions; one for the bulk and one for the clay analysis. The fraction used for the bulk analysis was rolled approximately 50 times to randomly orient the mineral grains before being scanned.

The clay fraction (less than 5 micrometer portion) was separated from the bulk sample using Stokes' Law for particle sedimentation. After an air dried scan was performed, the sample was allowed to interact with ethylene glycol vapors to induce swelling of susceptible clays. A second scan was run and the air-dried and glycolated patterns compared to determine which, if any, expandable clays are present. The abundances of the clay minerals were determined from the Reitveld refinement of the bulk scans. The results of the XRD analyses are presented in tables 3.1 to 3.3. XRD patterns for the clay fractions from each sample are given in Appendices D to F.

Results

The rocks encountered in the wells have been affected by both tectonic and hydrothermal activity. The effects of this activity are discussed in the following sections. Particular emphasis was placed on the distribution of the clay minerals and vein assemblages. The clay minerals are sensitive to temperature, and because smectite and interlayered illite-smectite have high electrical conductivities, these minerals have a strong influence on the geophysical signatures of the reservoir rocks. The veins represent past and present zones of permeability and consequently, their distribution will reflect the distribution of fractures and faults.

Tectonic Alteration

Tectonic activity is represented by brecciation and shearing of the rocks. The degree of tectonic brecciation with respect to depth is shown in figures 3.1 to 3.3. Examples of brecciated rock are presented in figures 3.4 to 3.6. Comparison with figures 3.7 to 3.9 suggest that the degree of alteration, as represented by the abundance of clay minerals, and brecciation are interrelated. In general, regions of greater tectonic activity are also regions of greater hydrothermal alteration and veining. These are also the zones where present-day permeability may be enhanced. This relationship is particularly apparent in 33A-7, where zones of increased alteration are also represented by increases in brecciation and the extent of veining. Similar relationships are observed to varying degrees in 33A-7 ST-1 and 83-11.

Hydrothermal Alteration

The rocks of the Coso geothermal reservoir have undergone multiple episodes of metamorphism, intrusive activity and hydrothermal alteration. These events have produced a succession of

generally similar mineral assemblages that have been difficult to separate. Consequently no mineral assemblage diagnostic of modern geothermal activity has previously been recognized. Nevertheless, it has frequently been possible to separate at least two events, one related to early episodes of regional metamorphism and the other to the recent geothermal history of the field. This recent geothermal activity is best reflected in the distribution of the clay minerals and in fluid inclusion data obtained on quartz and calcite veins (Moore and others, 1989; Lutz and others, 1996). The age of the most recent activity is unknown, but ^{14}C dates on plant matter in a sinter deposit has yielded an age of 8537 $\pm$ 30 years BP (unpublished data of J. Moore).

The early metamorphic assemblage is characterized by intergrowths of epidote, plagioclase, hornblende and biotite. This mineral assemblage is typical of the diorite in the sampled intervals. This assemblage is interpreted to reflect regional greenschist facies metamorphism of the rocks. The metamorphic assemblage was subsequently altered to chlorite, illite, titanite, epidote, quartz and calcite and cut by veins of quartz and epidote (figs. 3.6 and 3.10). Illite and chlorite are stable only at temperatures in excess of 225^{o}C, whereas epidote is indicative of temperatures greater than 240 to 260^{o}C (Browne, 1978; Henley and Ellis, 1983; Reyes, 1990). These minerals are found at all depths, from the surface downward. Thus they must have formed, at least in part, prior to the onset of modern geothermal activity, perhaps in response to waning temperatures during the later stages of regional metamorphism or to emplacement of younger intrusions.

The occurrence of epidote in the rhyolite in 33A-7 ST-1 provides compelling evidence of a second, relatively recent high-temperature geothermal event on the western flank of the geothermal system (figs. 3.11 and 3.12). As discussed below, vein assemblages consisting of various proportions of epidote, adularia, prehnite (one sample), chlorite, quartz, calcite and fluorite (one sample) are also interpreted to be geothermal in age even though their ages relative to the rhyolite cannot be determined from crosscutting relationships. Many of these veins have significant porosity, consistent with, but not proving, emplacement at relatively shallow depths.

Epidote veins are common throughout 33A-7 and 33A-7 ST-1 but only occur sporadically in 83-11. A significant percentage of these epidote-bearing veins also contain adularia (figs. 3.13 to 3.17). In contrast, adularia veins in 83-11 are frequently monomineralic but monomineralic veins also occur in the 33A-7 wells (figs. 3.18 and 3.19). The presence of vein adularia is significant. Adularia veins are rare in other parts of the field and thus are unlikely to be related to pre-rhyolite intrusive events. Their occurrence with epidote implies that the epidote is also geothermal in origin.

Adularia veins are common in many geothermal systems, primarily within the propylitic zone where temperatures exceed approximately 250^{o}C, although it can form at lower temperatures, perhaps as low as 150^{o}C (Henley and Ellis, 1983). Browne (1978) noted that adularia is common in zones of high permeability and that precipitation of vein adularia frequently results from boiling. At Broadlands-Ohaaki, the highest concentrations of adularia are found in upflow zone where temperatures exceed 250^{o}C (Simmons and Browne, 2000). $^{40}Ar/^{39}Ar$ spectrum dating can be used to determine the age of adularia deposition.

Prehnite occurs in the adularia vein from 8100 ft in 33A-7 ST-1 (fig. 3.20). Prehnite, like adularia is common in geothermal systems worldwide but was not previously indentified in wells

from the Coso field. It tends to form at lower temperatures than those required to stabilize epidote

Quartz veins were observed in 33A-7 ST-1 and 83-11 in the diorite and rhyolite. Quartz occurs with epidote in vugs in the rhyolite (fig. 3.11), as monomineralic veins of unknown age (fig. 3.21), as a late stage mineral in epidote + quartz veins (fig. 3.22) and in quartz + calcite veins (fig. 3.23) where it was deposited earlier than the calcite. Moore and others (1989) and Lutz and others (1996) demonstrated, through fluid inclusion studies, that quartz veins related to geothermal activity were widely distributed throughout the Coso geothermal field. These geothermal veins provide a record of low- to moderate-salinity waters (up to several weight percent NaCl) trapped at temperatures ranging from 100^{o} to greater than 325^{o}C. They document temperature-salinity relationships and patterns of fluid flow that mimic those expected based on the distributions of downhole temperatures and produced fluids. Although no fluid inclusion data was obtained on quartz veins in 33A-7 ST-1 their occurrence in the rhyolite clearly indicates an origin related to recent geothermal activity.

Calcite is invariably a late stage mineral in the veins. It forms monomineralic veins and fills vugs in veins containing epidote, adularia, quartz, and chlorite (figs. 3.24 to 2.30). Locally, the calcite veins are sheared indicating tectonic activity continued after their formation (fig. 3.31). Calcite from 9710 ft in 33-7 contains fluid inclusions consistent with modern downhole temperatures and salinities (Moore, unpublished report to the Coso Operating Co.). Primary fluid inclusions in the calcite yielded homogenization temperatures (minimum trapping temperatures) of 257^{o} to 262^{o}C and salinities of 0.5 weight percent.

Calcite has retrograde solubility and consequently will precipitate in response to heating of downward percolating waters. Calcite will also deposit in response to boiling, but boiling will commonly produce intergrowths of calcite and quartz and bladed calcite crystals. The textural relationships in the samples studied indicate that calcite was deposited after the other minerals, except fluorite, and that heating of inflowing bicarbonate-rich steam-heated waters and not boiling was the mechanism responsible for calcite deposition.

Fluorite was the last mineral to be deposited. It encapsulates both epidote and calcite. It is rarely observed at Coso and was only seen in one sample in this study at 9160 ft in 33A-7 ST-1. This samples consists dominantly of rhyolite.

The clay minerals deposited in the matrix of the rocks include illite, interlayered illite-smectite, rarely interlayered chlorite-smectite and chlorite. Interlayered illite-smectite is an intermediate phase between smectite, which first becomes stable at ~180^{o}C and illite, the stable mica above 225^{o}C (Henley and Ellis, 1983; Reyes, 1990). As the temperature increases above ~180^{o}C, the smectite content of the clay progressively decreases. Interlayered chlorite-smectite displays a similar change in composition with temperature. Smectite and smectite-bearing interlayered clays are electrically conductive and thus will affect the response of the rocks to electrical geophysical surveys. Significant concentrations of interlayered illite-smectite are found mainly above 7380 ft in 33A-7 and 7780 ft in 83-11. Interpretation of the XRD patterns indicates this interlayered clay has a high percentage of smectite, generally above 50%.

In many geothermal reservoirs, interlayered clay minerals are present to depths and temperatures beyond their commonly accepted stability ranges. This is also the case at Coso, where trace amounts to a few percent interlayered illite-smectite are found throughout the depth intervals studied. The reason for the persistence of these clays is not known. However, it is possible they are relict phases that formed when temperatures were lower and were subsequently unable to interact with the thermal fluids as temperatures increased because of low permeabilities in the surrounding rock. The small amounts of these clay minerals found in the deeper rocks is not expected to have a large effort on their electrical resistivites.

4.0. SUMMARY

The following conclusions can be drawn from this study.

1. The reservoir rocks in wells 33A-7 and 33A-7 ST-1 consist of diorite, granite and rhyolite. Rhyolite is uncommon in other parts of the field. The rhyolite displays devitrification textures and, in places, is silicified. The rhyolite is interpreted to represent dikes recently emplaced along major fracture zones.
2. The veins found in the rocks display textures and mineral assemblages not frequently observed in the Coso reservoir. These veins contain epidote, adularia, chlorite, quartz, calcite and rarely prehnite and fluorite and are interpreted to have been deposited during recent geothermal activity. Significant concentrations of adularia veins have not been observed in other parts of the field. Epidote is indicative of temperatures exceeding 250^{o}C. It occurs in veins and vugs in the rhyolite.
3. Veins containing significant porosity are widespread in the sampled intervals of 33A-7 and 33A-7 ST-1. Veins in 83-11 rarely contain vugs.
4. Adularia and epidote veins are common in the high temperature portions of many geothermal systems. The most likely mechanism for adularia deposition is boiling of the geothermal fluids. Consequently adularia veining is often taken as a good indicator of permeability. Adularia may be enriched in the upflow zones of geothermal systems.
5. The mineral paragenesis of the veins can be summarized as follows (upper case X indicates the phase is abundant; lower case x refers to trace amounts) :

Epidote	X				
Adularia	X				
Chlorite	x				
Quartz	x	x			
Prehnite			x		
Calcite				X	
Fluorite					x

6. The degree of alteration is best represented by the abundance of the clay minerals, illite, chlorite and interlayered illite-smectite interlayered and chlorite-smectite.

7. The adularia veins in 33A-7 are most abundant in the more strongly altered and brecciated rocks. In 33A-7 ST-1, porous adularia veins occur primarily at depths above the rhyolite.
8. Calcite is interpreted to have formed in response to heating of downward percolating bicarbonate-rich waters. These waters may have formed when CO_2 released by the upward flowing boiling thermal waters dissolved in the shallow overlying waters.
9. Taken together, the presence of adularia veins, partially filled veins, tectonic breccias and clay alteration may be good indicators of permeability on the west flank. Additional petrographic studies of other wells and depth intervals chould be conducted to determine if the zone of alteration and rhyolite dikes sampled in 33A-7, 33A-7 ST-1 and 83-11 are part of a major fracture zone on the west flank of the field.

5.0. REFERENCES

Browne, P. R. L., 1978, Hydrothermal alteration in active geothermal fields: Annual reviews in Earth and Planetary Science, v. 6, p. 229-250.

Henley, R. W., and Ellis, A. J., 1983, Geothermal systems ancient and modern: A geochemical review: Earth-Science Reviews, v. 19, p. 1-50.

Lovera, O. M., Richter, F. M. and Harrison, T. M., 1991, Diffusion domains determined by ^{39}Ar release step-heating: Journal of Geophysical Research, v. 96, p.2057-2069

Lutz, S. J., Moore, J. N., and Copp, J. F., 1996, Integrated hydrothermal alteration and fluid inclusion investigations of the Coso geothermal System: Twenty-first Workshop on Geothermal Reservoir Engineering, Stanford University, p. 187-194.

Moore, J. N., Adams, M. C., Bishop, B. P., and Hirtz, P., 1989, A fluid flow model of the Coso geothermal system, California: Data from fluid chemistry and fluid inclusions: Fourteenth Workshop on Geothermal Reservoir Engineering, Stanford University, p. 139-144.

Moore, J., Norman, D, and Adams, A, 2004, Thermal and chemical history of the eastern side of the Coso geothermal field: unpublished report to the Geothermal Program Office, U.S. Navy

Reyes, A. G., 1990, Petrology of Philippine geothermal systems and the application of alteration mineralogy to their assessment: Journal of Volcanology and Geothermal Research, v. 43, p.279-309.

Simmons, S., and Browne, P. R. L., 2000, Hydrothermal minerals and precious metals in the Broadlands-Ohaaki geothermal system: implications for understanding low-sulfidation epithermal environments: Economic Geology, v. 95, p. 971-999.

Table 3.1. Results of the bulk Rietveld refinements for well 33A-7 listed by sample interval (ft) given in weight percent of sample. Tr = trace amount.

		Chlorite	Chlorite/Smectite	Illite	Illite/Smectite	Plagioclase	Quartz	K-feldspar	Calcite	Titanite	Epidote	Biotite	Hornblende	Pyrite
6960	6970	5.1		3.3	Tr	53.1	15.1	6.8	0.4	1.1	1.0	7.1	6.9	
7040	7050	6.9		4.5		49.3	3.8	5.2		1.2	2.7	12.5	13.9	
7060	7070	18.0			4.9	34.4	5.8	3.0	1.1	1.2	5.1	7.3	19.2	
7120	7130	16.8			2.9	39.7	7.7	2.1			7.0	12.1	11.7	
7190	7200	8.9			5.5	41.7	16.7	12.0	1.9		2.6	2.5	8.3	
7230	7240	9.6			3.8	47.8	1.7	2.6			1.5	7.5	25.5	
7270	7280	19.5		1.3		44.1	0.6	3.9	0.3	1.2	2.8	4.0	22.3	
7340	7350	20.1			3.6	44.4	3.8	3.5	0.5	1.1	3.3	6.6	13.1	
7370	7380	11.1			4.7	49.6	1.4	4.8	3.4	1.9	3.7	4.2	15.0	
7440	7450	4.9		6.8	Tr	48.9	0.3	2.1			2.9	6.0	28.2	
7460	7470		10.8	1.1	Tr	50.8	1.2	4.9		1.6	5	3.7	21.0	
7510	7520	7.0		8.3	Tr	53.6	1.0	3.8		1.2	2.4	4.7	18.0	
7580	7590	9.2		3.2	Tr	55.8	1.0	4.8	1.0	1.1	3.3	4.3	16.3	
7620	7630	11.8		3.9	Tr	55.1	4.5	2.6	1.3		2.7	5.4	12.7	
7680	7690	2.6		2.8	Tr	45.1	23.4	18.8		1.9	1.9	2.6	1.0	
7780	7790	2.9		2.7		50.6	20.7	14.7		0.9	1.9	3.1	2.5	
7830	7840	1.8		1.9	Tr	44.1	21.6	22.6		1.5	0.7	2.9	2.8	
7880	7890	4.4		2.5	Tr	52.4	17.3	10.9		1.3	2.0	4.1	5.1	
7940	7950		6.6	4.4	Tr	44.2	2.5	2.8			3.4	3.2	32.9	
7990	8000	2.7		3.5	Tr	36.7	22.1	18.2			2.0	1.7	13.2	
8020	8030	3.1		2.4	Tr	49.9	2.5	4.8			2.4	3.4	31.3	
8080	8090	2.8		1.8	Tr	45.3	12.8	12.0		1.4	2.7	4.1	17	
8110	8120	1.1		1.9	Tr	38.3	32.0	22.4			1.1	0.5	2.6	
8260	8270	3.3		3.3	Tr	45.7	18.6	13.9	0.2	1.0	2.3	3.0	8.7	
8300	8310	6.7		3.6	Tr	50.5	4.2	4.5	0.5	1.7	4.9	4.5	17.4	1.5

Table 3.2. Results of the bulk Rietveld refinements for well 33A-7 ST-1 listed by sample interval (ft) given in weight percent of sample. Tr = trace amount.

		Chlorite	Illite	Illite/Smectite	Plagioclase	Quartz	K-feldspar	Calcite	Titanite	Epidote	Biotite	Hornblende	Pyrite
8100	8110	7.1	3.8	Tr	52.4	2.5	6.6		0.6	2.6	2.8	21.7	
8210	8220	3.1	3.1		48.5	5.6	4.2		0.5	2.2	3.5	29.2	
8290	8300	2.4	1.5		46.1	10.0	6.5		0.9	1.2	3.6	27.9	
8400	8410	1.9	1.1	Tr	56.5	10.2	7.5	0.1	1.2	1.5	4.4	15.6	
8450	8460	4.8	1.5	Tr	47.5	8	8.2		0.9	2.1	3.0	24.0	
8530	8540	2.4	2.8	Tr	48.6	18.4	14.7		1.6	0.9	4.5	6.0	
8570	8580	4.0		3.3	58.3	12.5	11.0		1.3	0.7	5.1	3.7	
8650	8660	8.0	3.9	Tr	66.3	3.2	8.7		1.9	2.4	5.4		0.5
8710	8720	6.6	2.6	Tr	51.7	1.3	3.9		1.5	2	4.3	26.1	
8780	8790	7.8	6.4	Tr	41.8	4.1	5.2		1.2	3.3	2.9	27.4	
8880	8890	5.7	3.0	Tr	43.0	1.6	2.1		1.0	3.9	4.9	34.8	
9000	9010	3.2	3.6	Tr	57.7	1.7	2.8		0.6	1.3	7.4	21.7	
9050	9060	4.4	3.5	Tr	60.5	0.6	2.9		0.5	0.8	6.4	20.4	
9160	9170	1.9	3.0		39.3	28.1	19.6		0.3	2.2	2.5	3.0	
9260	9270	0.4	2.1		35.7	33.8	24.5		0.2	1.4	0.1	1.7	
9300	9310	0.7	3.3		36.5	31.5	23.3		0.3	0.9	0.9	2.5	
9410	9420	1.2	3.2	Tr	33.2	31.0	25.3		0.2	2.4	0.5	3.0	
9490	9500	1.9	2.9	0.4	31.7	24.0	21.2		0.4	4.4	1.9	11.2	
9510	9520	2.2	2.6	1.2	33.8	28.5	22.1		1.3	3.0	1.5	3.9	
9600	9610	6.3	6.9	0.3	32.1	7.8	10.8		1.2	5.9	1.1	27.6	
9720	9730	1.0	2.5		30.9	28.5	33.1		0.9	0.4	0.7	1.8	
9950	9960	2.5	3.1	Tr	41.6	16.0	11.8		1.4	1.2	3.2	19.2	
10020	10030	3.4	3.8	Tr	44.6	10.3	6.8		0.6	1.6	3.5	25.4	
10090	10100	2.0	3.0	Tr	39.3	16.2	13.0		0.5	1.0	2.1	23.1	
10160	10170	1.4	2.9	Tr	40.1	21.3	14.9		0.5	0.9	1.5	16.4	

Table 3. 3. Results of the bulk Rietveld refinements for well 83-11 listed by sample interval (ft) given in weight percent of sample. Tr = trace amount.

		Chlorite	Illite	Illite/Smectite	Plagioclase	Quartz	K-feldspar	Calcite	Titanite	Epidote	Biotite	Hornblende	Pyrite
6780	6790	3.5	6.2	Tr	49.8	18.7	6.5	2.1	1.0	2.5	5.5	2.8	1.4
6820	6830	3.3		3.9	52.0	6.4	1.9	0.5	1.9	1.7	6.7	21.8	
6880	6890	3.9		2.9	54.5	14.6	4.5	2.5	1.1	3.3	7.0	5.8	
6920	6930	2.1	2.6	Tr	57.2	13.8	4.4	0.4	0.8	2.1	7.1	9.5	
6960	6970	2.0	2.2	Tr	53.2	18.4	9.1	1.7	1.4	1.7	4.5	6.0	
7020	7030	4.2	2.2	Tr	51.3	10.1	4.8	0.7	1.1	3.0	6.7	15.9	
7070	7080	5.2		2.5	53.3	2.1	3.0	0.8	1.8	1.4	8.5	21.3	
7140	7150	3.8		3.8	59.4	1.1	4.1	0.4	2.1	2.9	11.2	11.3	
7160	7170	5.4	3.4		60.3	0.9	6.5	0.5	3.3	2.7	6.1	11.1	
7200	7210	4.5		3.1	42.6	1.0	9.0	1.2	2.9	3.6	6.1	26.2	
7230	7240	5.1	2.6	Tr	51.2	1.8	3.4	0.9	2.7	2.5	5.9	24.0	
7250	7260	5.7		3.0	53.5	1.7	2.7	0.5	1.3	1.7	6.7	23.3	
7310	7320	5.1		2.8	54.2	6.2	3.8	0.9	1.8	3.1	6.4	15.6	
7390	7400	6.6		6.1	44.2	10.5	4.2	1.4	0.9	2.7	4.0	19.6	
7430	7440	1.9	5.1	Tr	41.2	26.5	15.2	0.3	0.7	1.8	2.3	5.0	
7490	7500	4.2		2.9	59.1	6.2	4.9	0.5	1.5	0.9	6.1	13.7	
7540	7550	3.6		3.6	62.9	5.9	2.4	0.1	1.2	1.2	7.0	12.1	
7590	7600	10.5	3.3	Tr	56.4	8.7	8.8	1.2	1.3	0.6	2.5	6.8	
7620	7630	12.5		8.3	42.0	12.0	6.3	4.0	0.7	1.3	2.8	10.1	
7680	7690	12.7	8.3		58.3	5.1	7.8	1.2	1.4	0.6	2.3	2.2	
7730	7740	6.2		4.2	54.1	4.2	3.8	0.8	1.5	2.3	7.9	14.9	
7780	7790	5.2	4.1	Tr	53.6	7.2	3.8	0.7	1.0	1.5	3.9	19.2	
7840	7850	2.5	4.0	Tr	51.1	9.1	3.5	0.3	1.3	3.0	3.5	21.6	
7860	7870	3.9	6.0	Tr	51.6	7.8	5.7	1.0	1.2	4.2	1.6	17.1	
7920	7930	6.0		5.4	53.7	4.9	1.9	0.8	1.1	1.5	4.5	20.1	
7990	8000	2.4	4.0	Tr	51.3	9.8	3.0	0.2	0.4	1.8	3.6	23.5	
8010	8020	2.1	2.4	Tr	50.7	16.1	8.2	0.2	2.0	2.1	6.1	10.1	
8050	8060	2.7	3.7	Tr	55.4	3.7	1.6	0.2	0.6	1.4	5.0	25.6	
8170	8180	2.3		1.7	59.1	2.0	2.3	0.3	0.5	1.1	3.7	27.1	
8200	8210	3.8	2.3	Tr	18.3	36.0	5.8	3.7	0.9	0.7	4.5	24.0	
8230	8240	4.2	3.7	Tr	60.0	3.3	4.2	0.2	0.9	0.8	4.9	17.8	
8270	8280	4.5		5.2	54.5	13.5	3.7	0.2	1.3	1.8	4.0	11.3	
8310	8320	6.5	2.4	Tr	55.9	5.5	5.7	2.6	0.8	1.2	5.5	14.0	
8350	8360	6.7	7.8	Tr	40.7	10.3	3.8	1.8	0.5	0.6	8.2	19.7	

Rock Type %

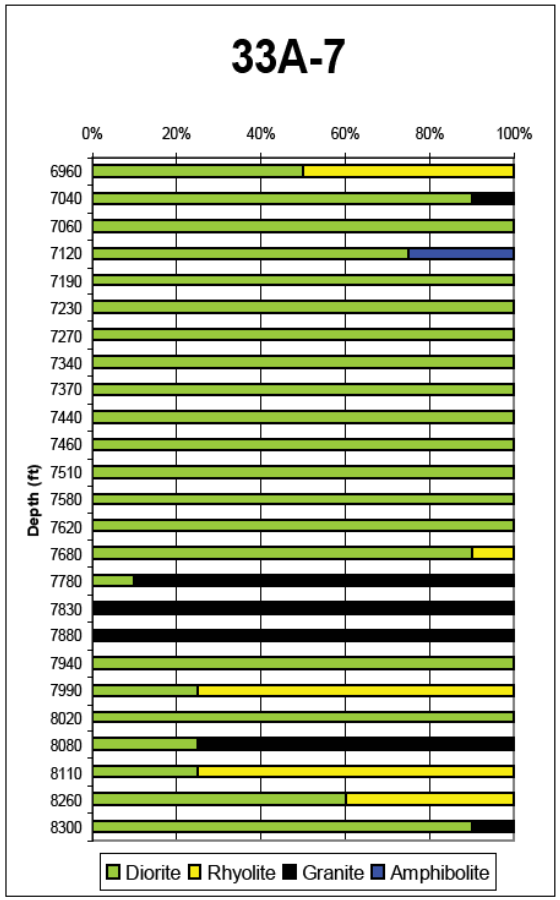
33A-7
0%
20%
40%
60%
80%
100%
Depth (ft)
6960
7040
7060
7120
7190
7230
7270
7340
7370
7440
7460
7510
7580
7620
7680
7780
7830
7880
7940
7990
8020
8080
8110
8260
8300
Diorite
Rhyolite
Granite
Amphibolite

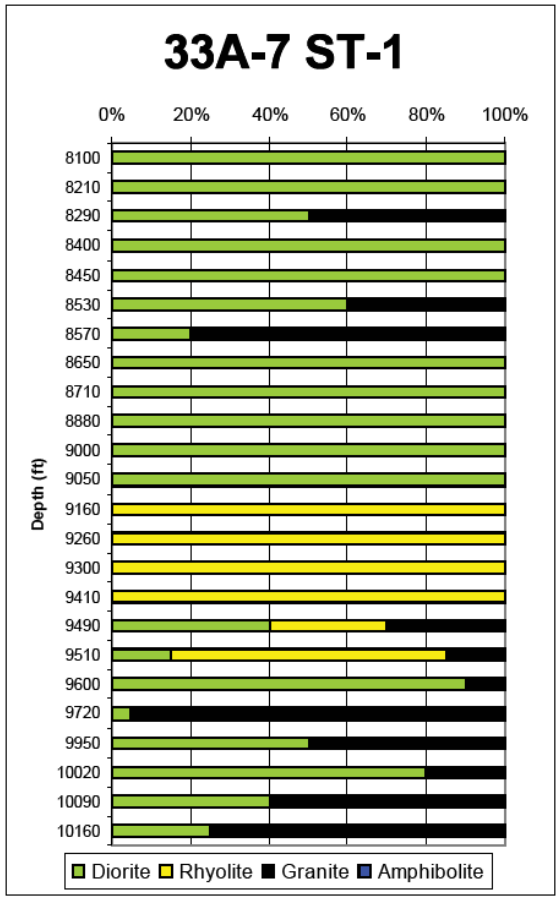
33A-7 ST-1
0%
20%
40%
60%
80%
100%
Depth (ft)
8100
8210
8290
8400
8450
8530
8570
8650
8710
8880
9000
9050
9160
9260
9300
9410
9490
9510
9600
9720
9950
10020
10090
10160
Diorite
Rhyolite
Granite
Amphibolite

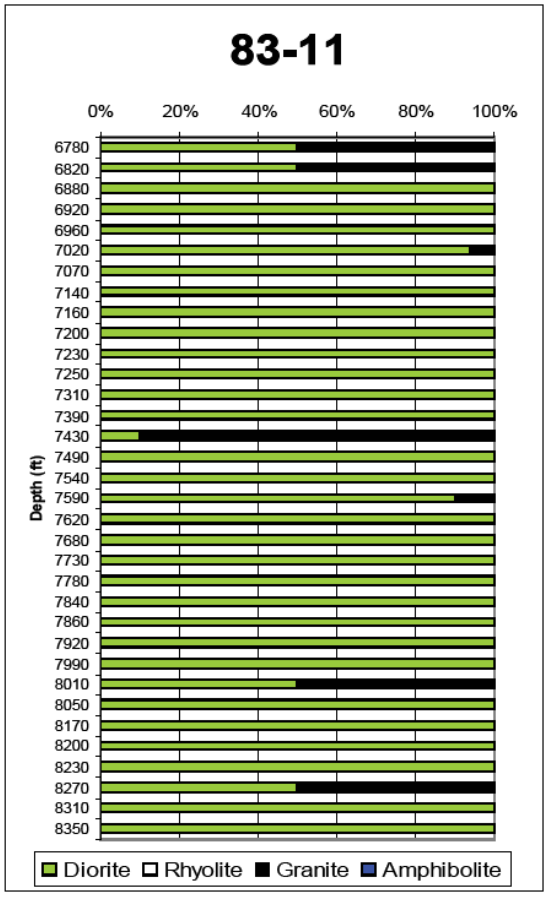
83-11
0%
20%
40%
60%
80%
100%
Depth (ft)
6780
6820
6880
6920
6960
7020
7070
7140
7160
7200
7230
7250
7310
7390
7430
7490
7540
7590
7620
7680
7730
7780
7840
7860
7920
7990
8010
8050
8170
8200
8230
8270
8310
8350
Diorite
Rhyolite
Granite
Amphibolite

Fig. 2.1 Diistribution of rock types in the wells studied.

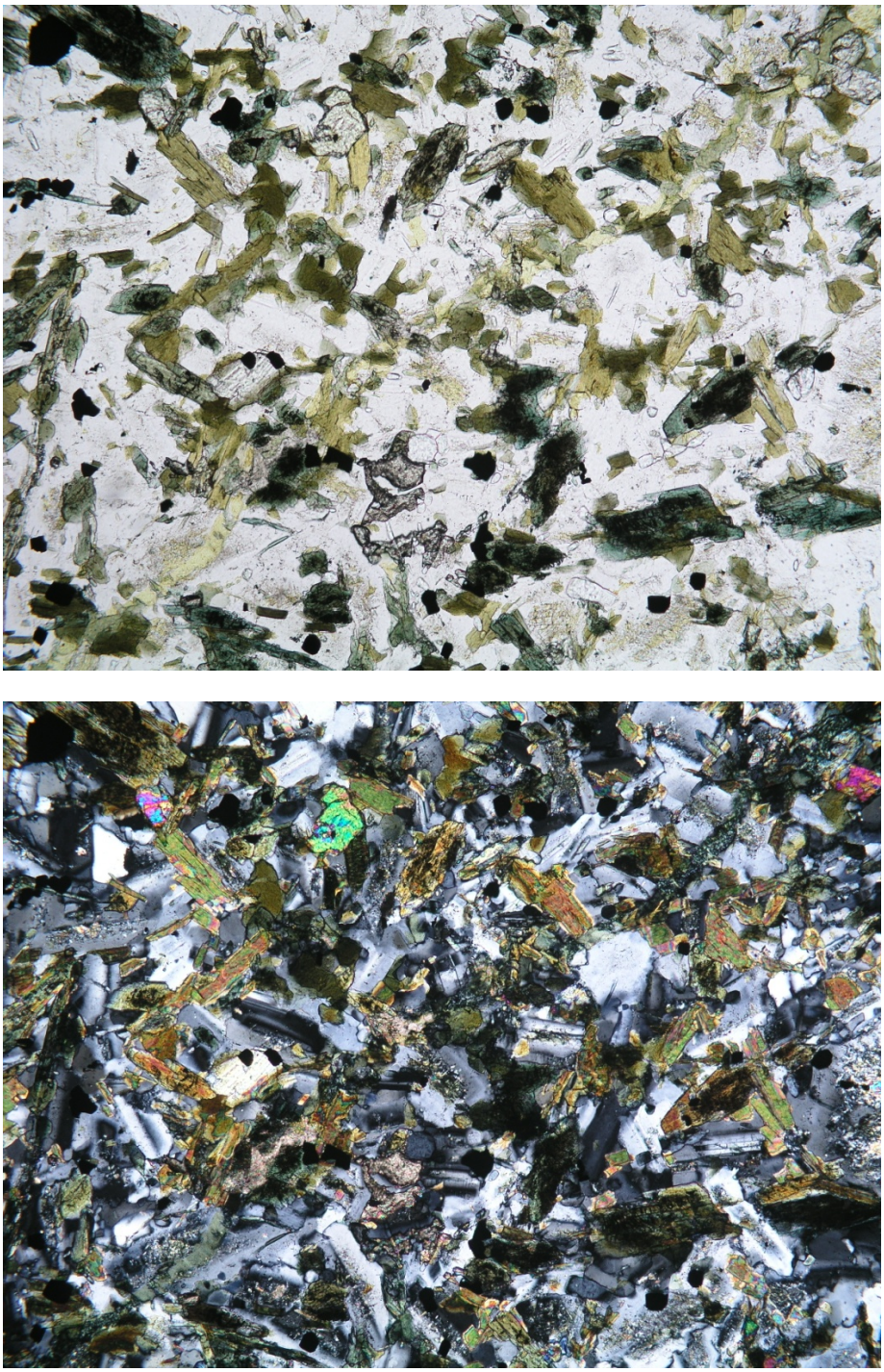

Fig. 2.2. Diorite consisting of plagioclase (colorless), biotite (brown), hornblende (green), epidote (yellow green, high relief), and pyrite (black). Plagioclase is partially altered to illite and K-feldspar (stained yellow). An adularia vein cuts the rock form lower left to upper right. Upper photomicrograph: plane polarized light; lower photomicrograph: crossed nicols. From 7070 ft in 83-11. Field of view is 1.6 mm across.

Note: Mineral descriptions in captions refer to the upper image in each figure.

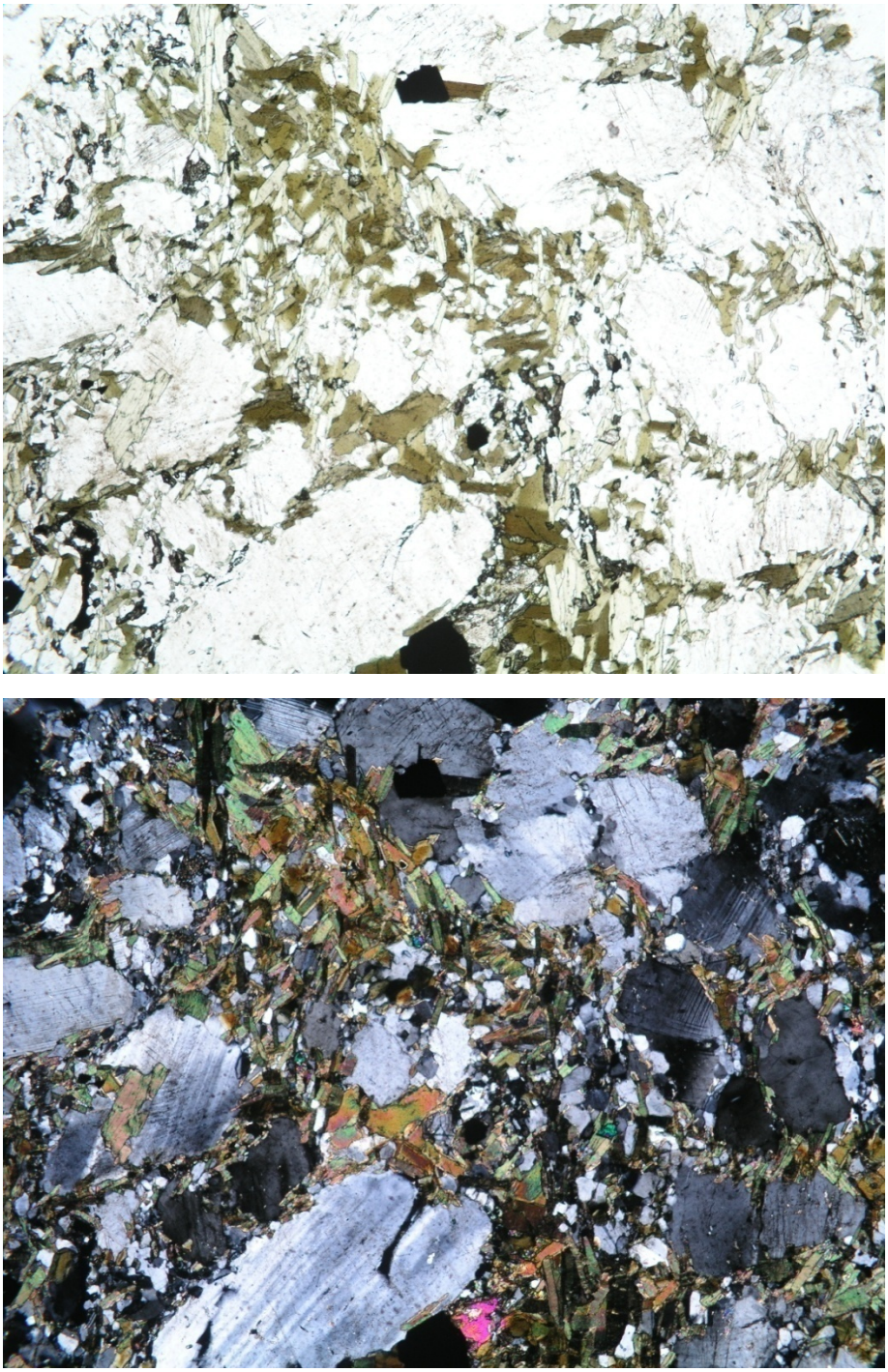

Fig. 2.3. Fresh diorite containing plagioclase (colorless) and biotite (light brown). Upper photomicrograph: plane polarized light; lower photomicrograph: crossed nicols. From 8710 ft in 33A-7ST-1. Field of view is 3.1 mm across.

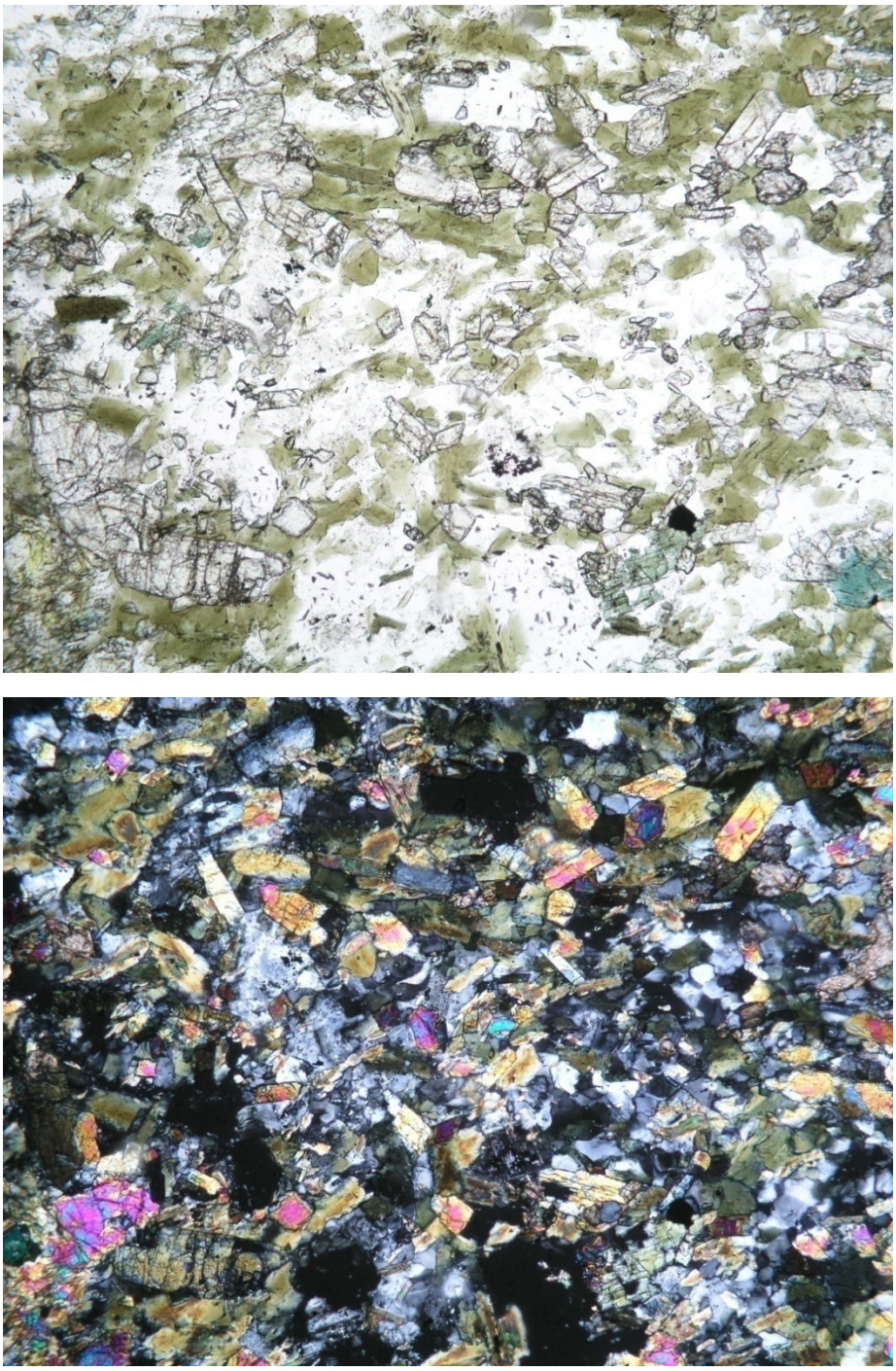

Fig. 2.4. Diorite, consisting of plagioclase (colorless, low relief), biotite altered to chlorite (green) and epidote (colorless to yellow-green, high relief). Upper photomicrograph: plane polarized light; lower photomicrograph: crossed nicols. From 7230 ft in 33A-7. Field of view is 1.6 mm across.

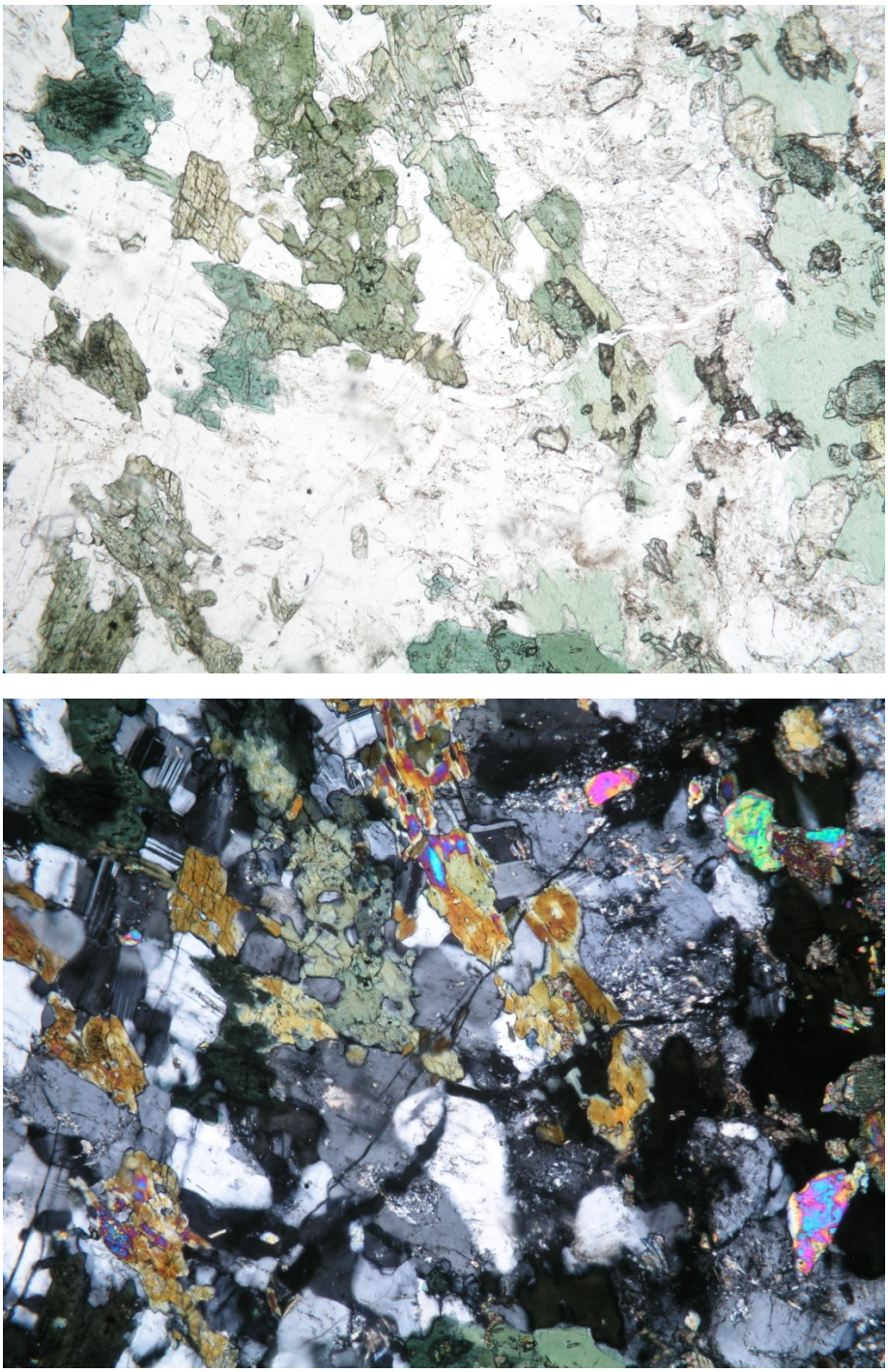

Fig. 2.5. Altered diorite containing hornblende (dark green), epidote (colorless to yellow-green, high relief) and chlorite (light green). Upper photomicrograph: plane polarized light; lower photomicrograph crossed nicols. From 8210 ft in 33A-7ST-1. Field of view is 3.1 mm across.Field of view is 1.6 mm across.

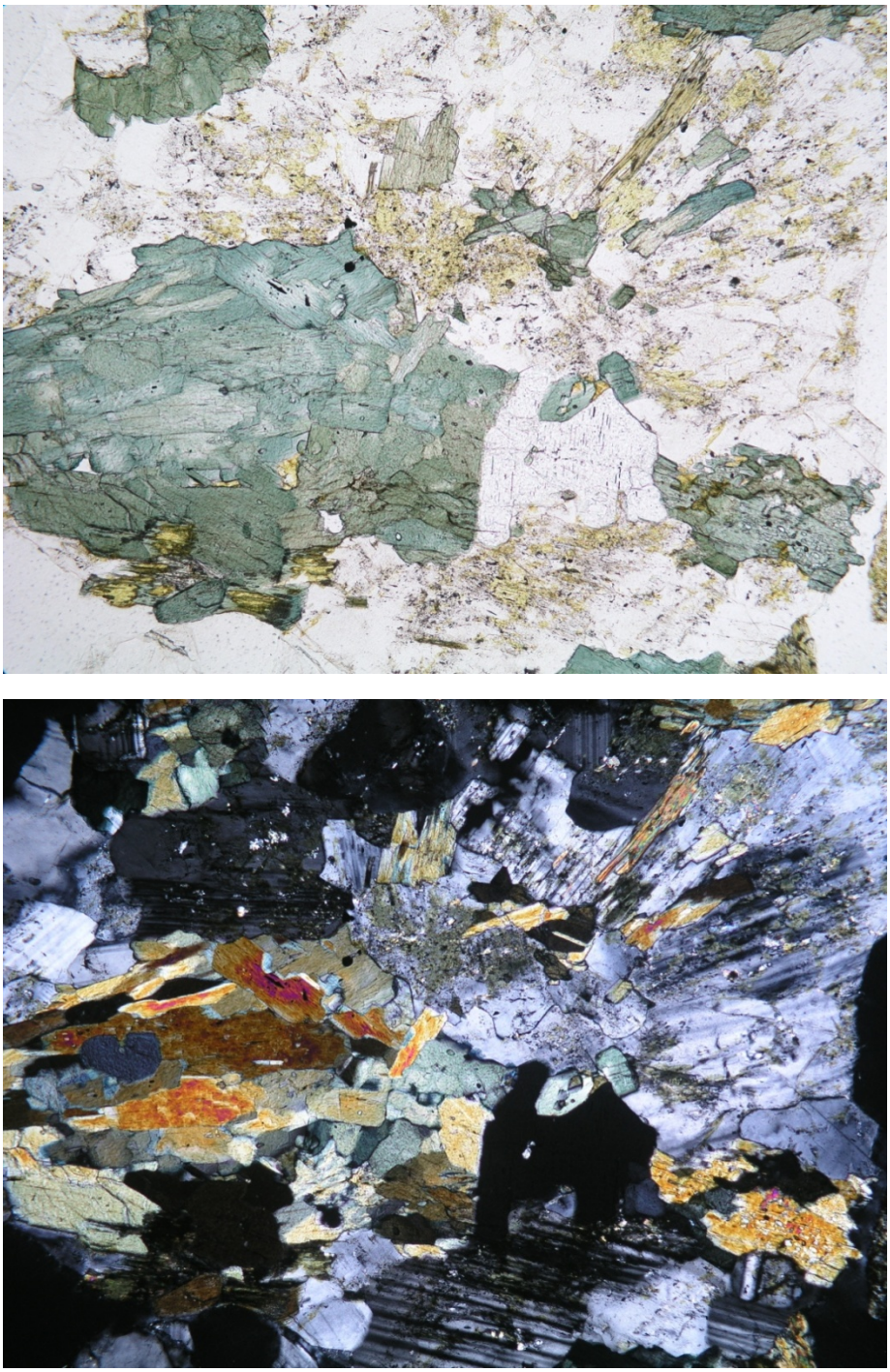

Fig. 2.6. Representative photomicrograph of diorite, containing hornblende (blue-green) and plagioclase partially replaced by K-feldspar (stained yellow). Upper photomicrograph: plane polarized light; lower photomicrograph: crossed nicols. From 9950 ft in 33A-7ST-1. Field of view is 1.6 mm across.

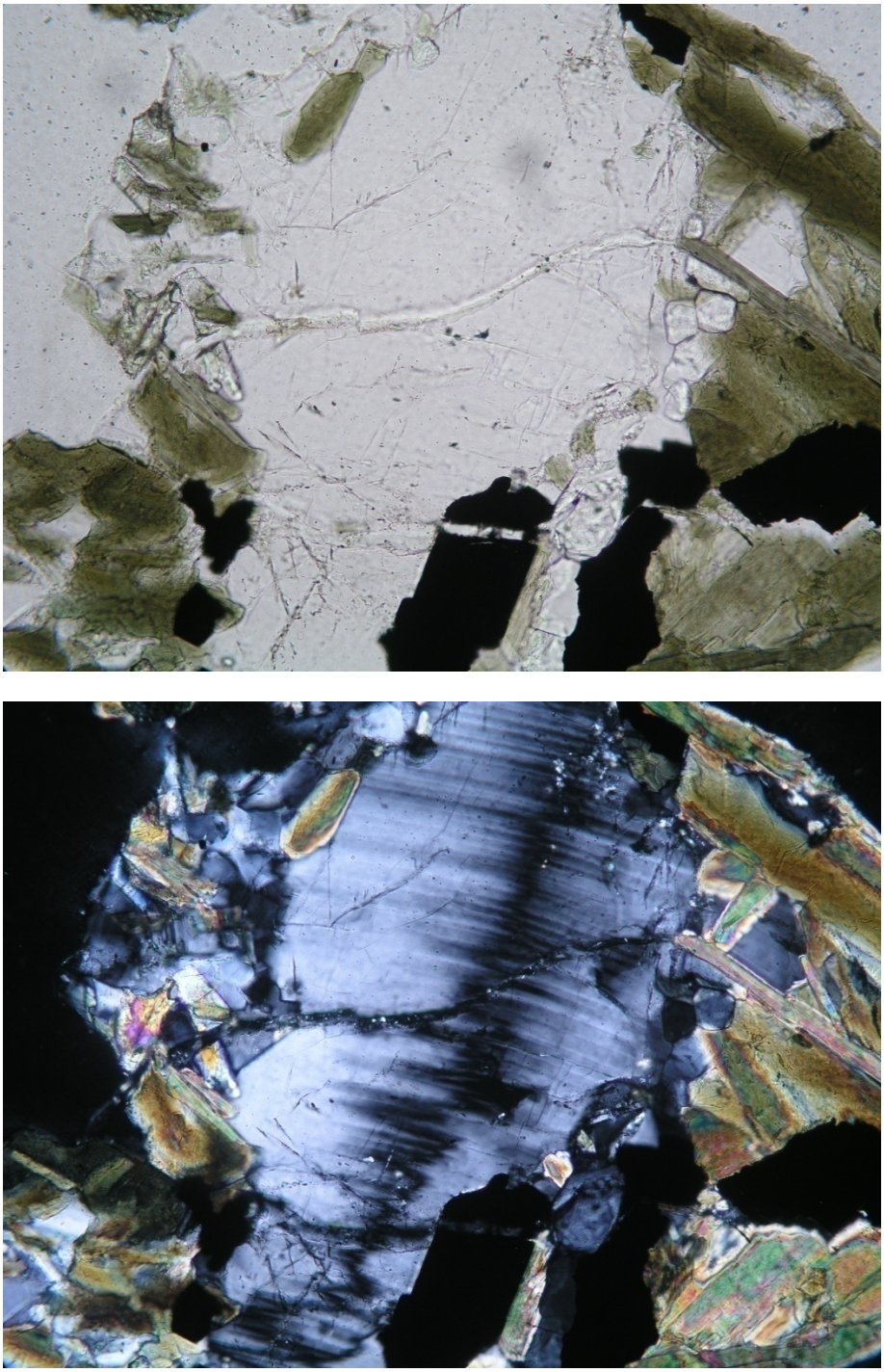

Fig. 2.7. Kinked plagioclase crystal surrounded by biotite. The twin planes in the plagioclase are distorted. Upper photomicrograph: plane polarized light; lower photomicrograph: crossed nicols. From a depth of 7580 ft in 33A-7. Field of view is 3.1 mm across. Field of view is 1.6 mm across.

Fig. 2.8. Amphibolite consisting of actiniolite (pale green), biotite (brown) and epidote (colorless to yellow-green, high relief). Upper photomicrograph: plane polarized light; lower photomicrograph: crossed nicols. From 7120 ft in 33A-7 ST-1. Field of view is 1.6 mm across.

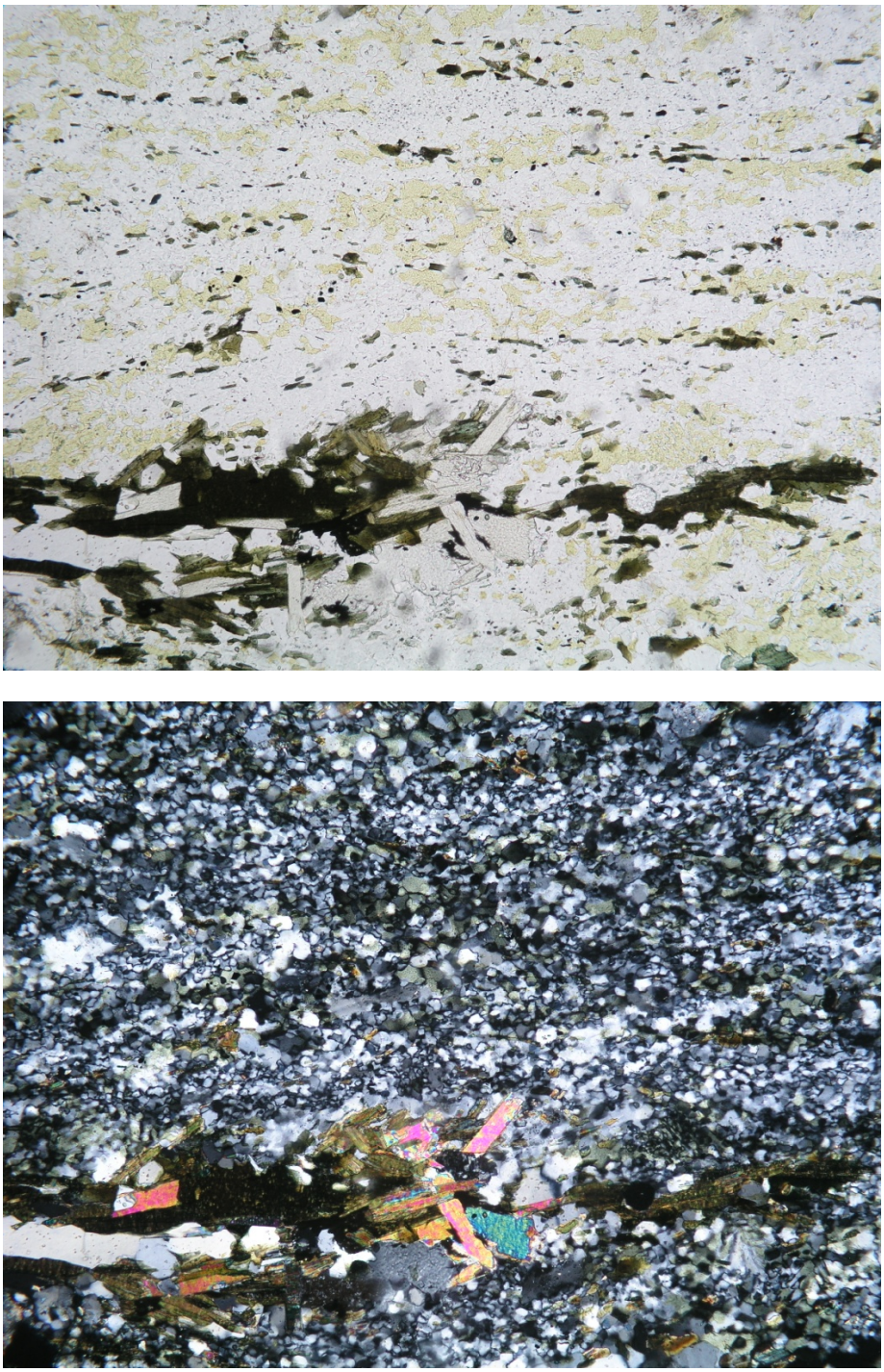

Fig. 2.9. Foliated, fine-grained granite containing K-feldspar (stained yellow), clear quartz and plagioclase, and biotite (brown to colorless). Upper photomicrograph: plane polarized light; lower photomicrograph: crossed nicols. From 7020 ft in 83-11. Field of view is 1.6 mm across.

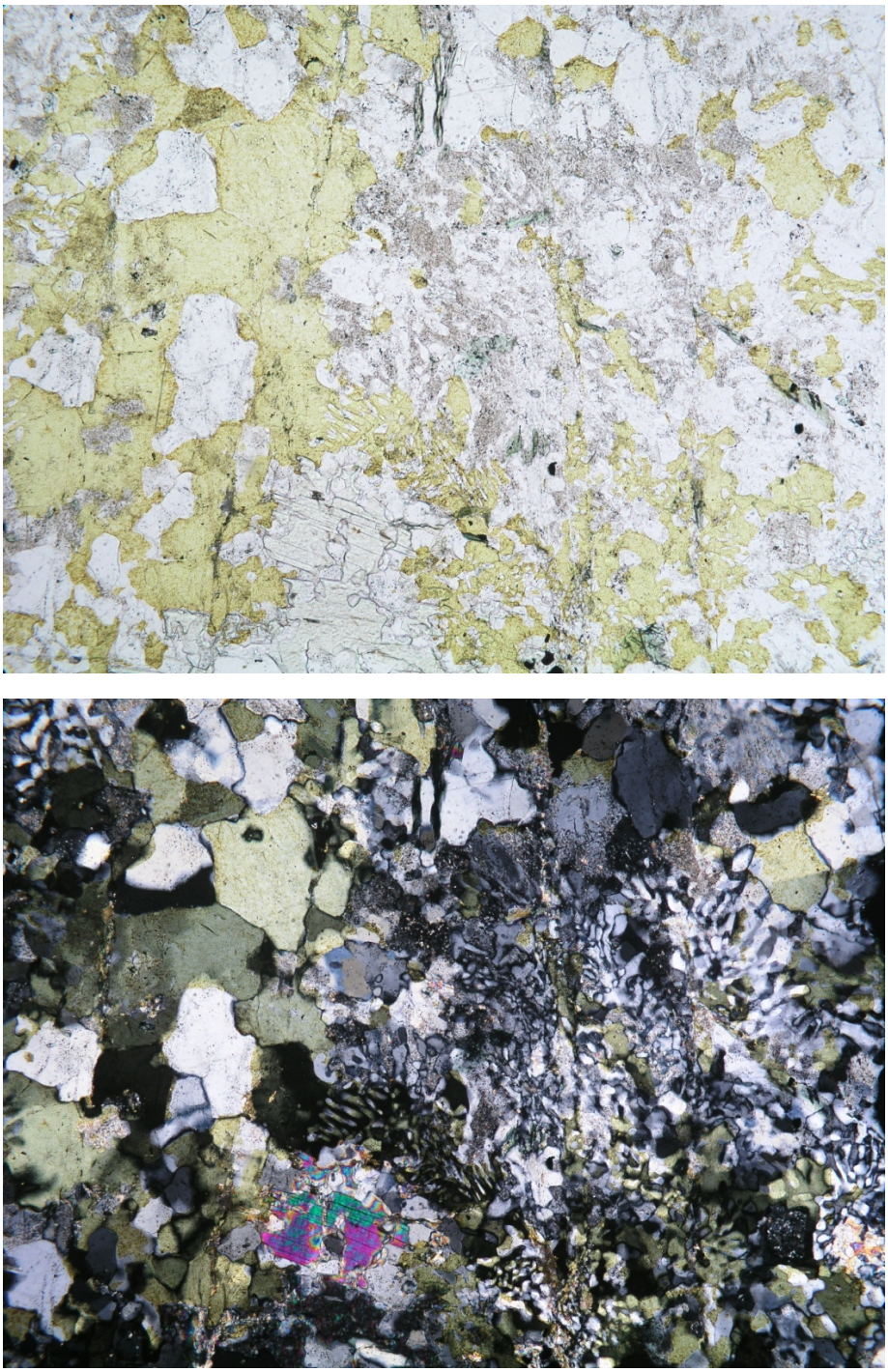

Fig. 2.10. Granite containing granophyric intergrowths of K-feldspar (stained yellow) and quartz in granite, with minor muscovite (bottom center). Upper photomicrograph: plane polarized light; lower photomicrograph: crossed nicols. From 8530 ft in 33A-7 ST-1. Field of view is 0.8 mm across.

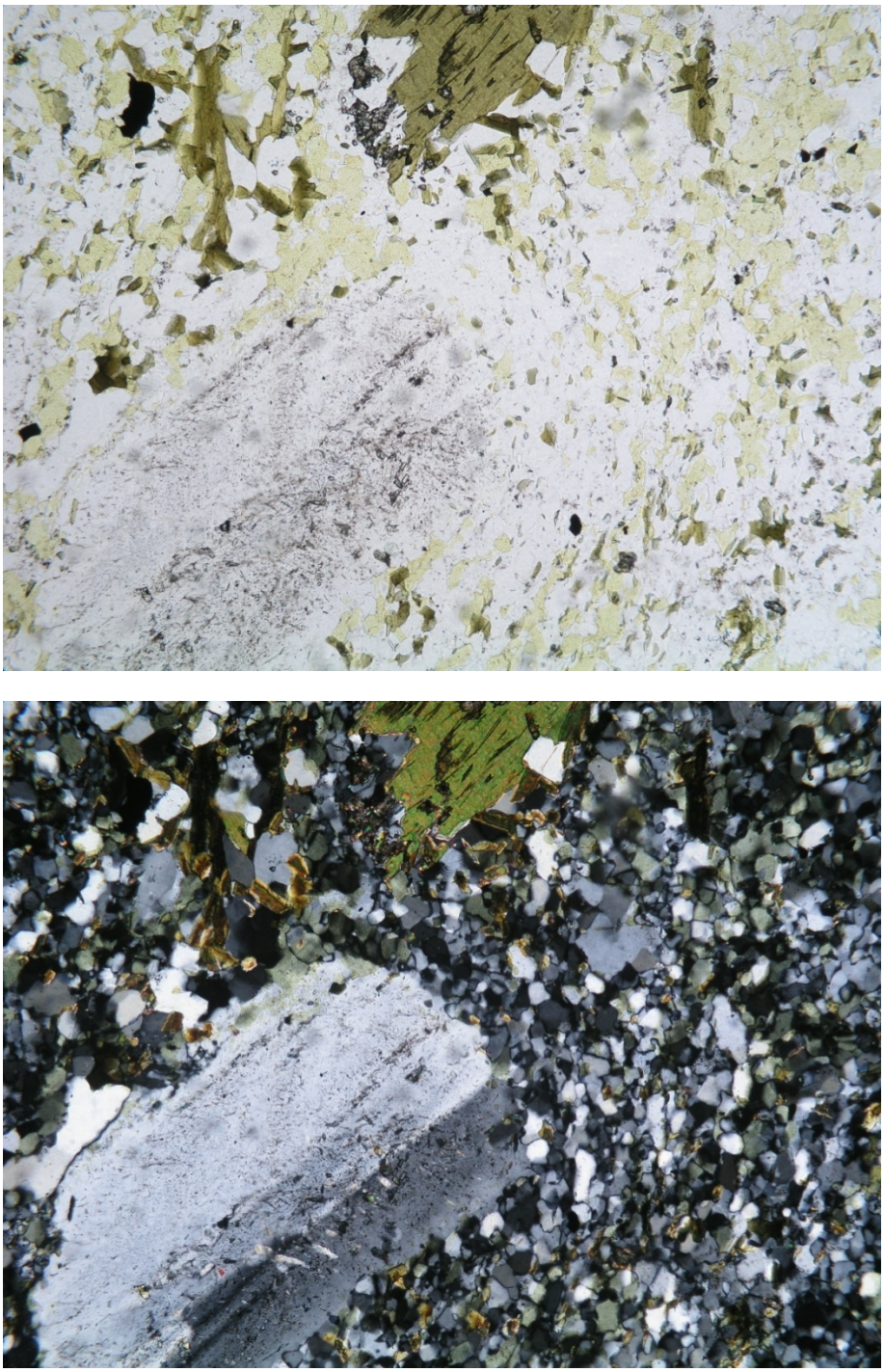

Fig. 2.11. Granite porphyry containing phenocrysts of plagioclase and biotite in a matrix rich in quartz and K-feldspar. Upper photomicrograph: plane polarized light; lower photomicrograph: crossed nicols. From 7830 ft in 33A-7. Field of view is 1.6 mm across.

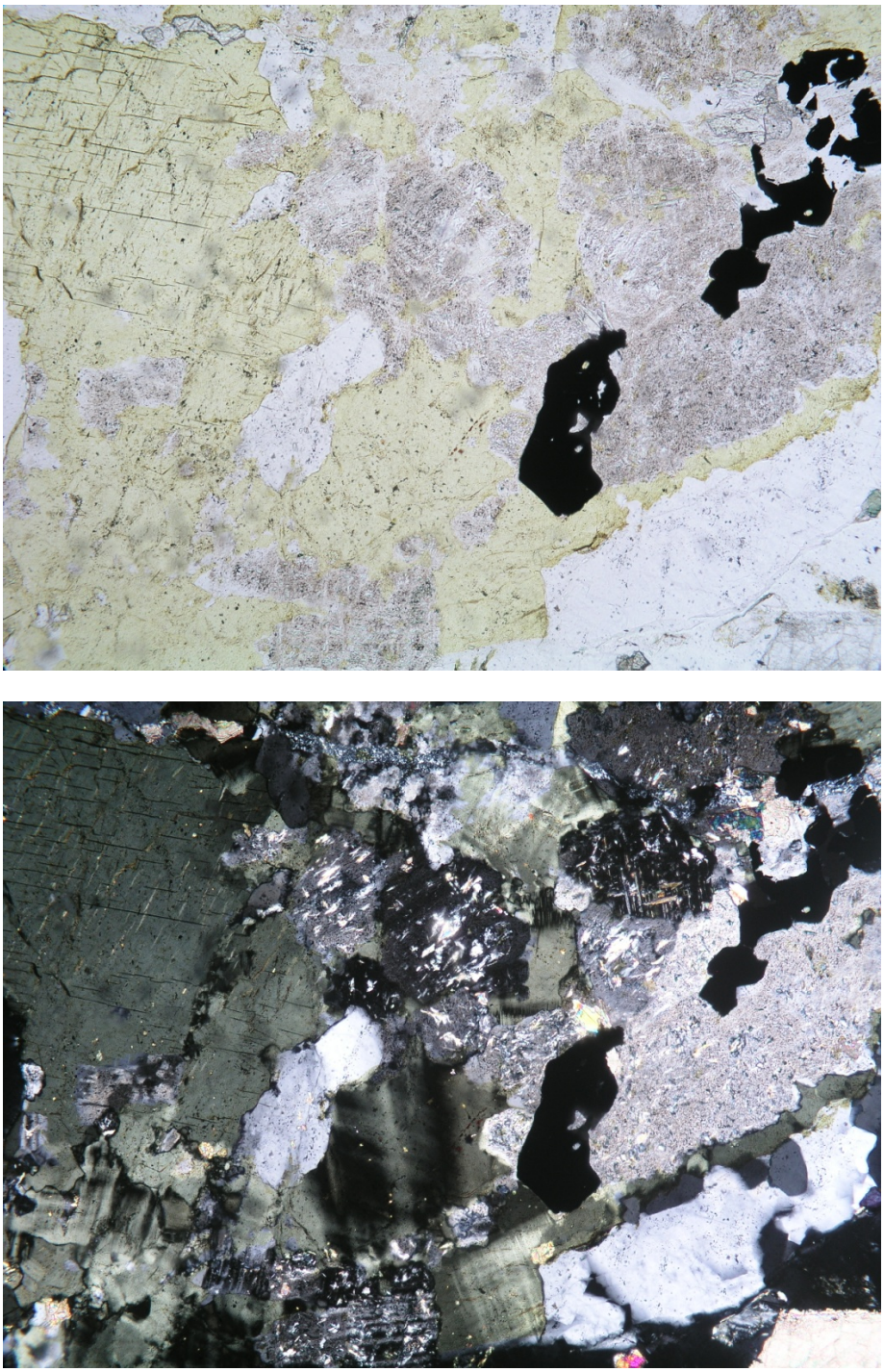

Fig. 2.12. Coarse-grained granite consisting of K-feldspar (stained yellow), plagioclase (grey due to alteration to illite), quartz (colorless)and magnetite (black). Upper photomicrograph: plane polarized light; lower photomicrograph: crossed nicols. From 7020 ft in 83-11. Field of view is 1.6 mm across.

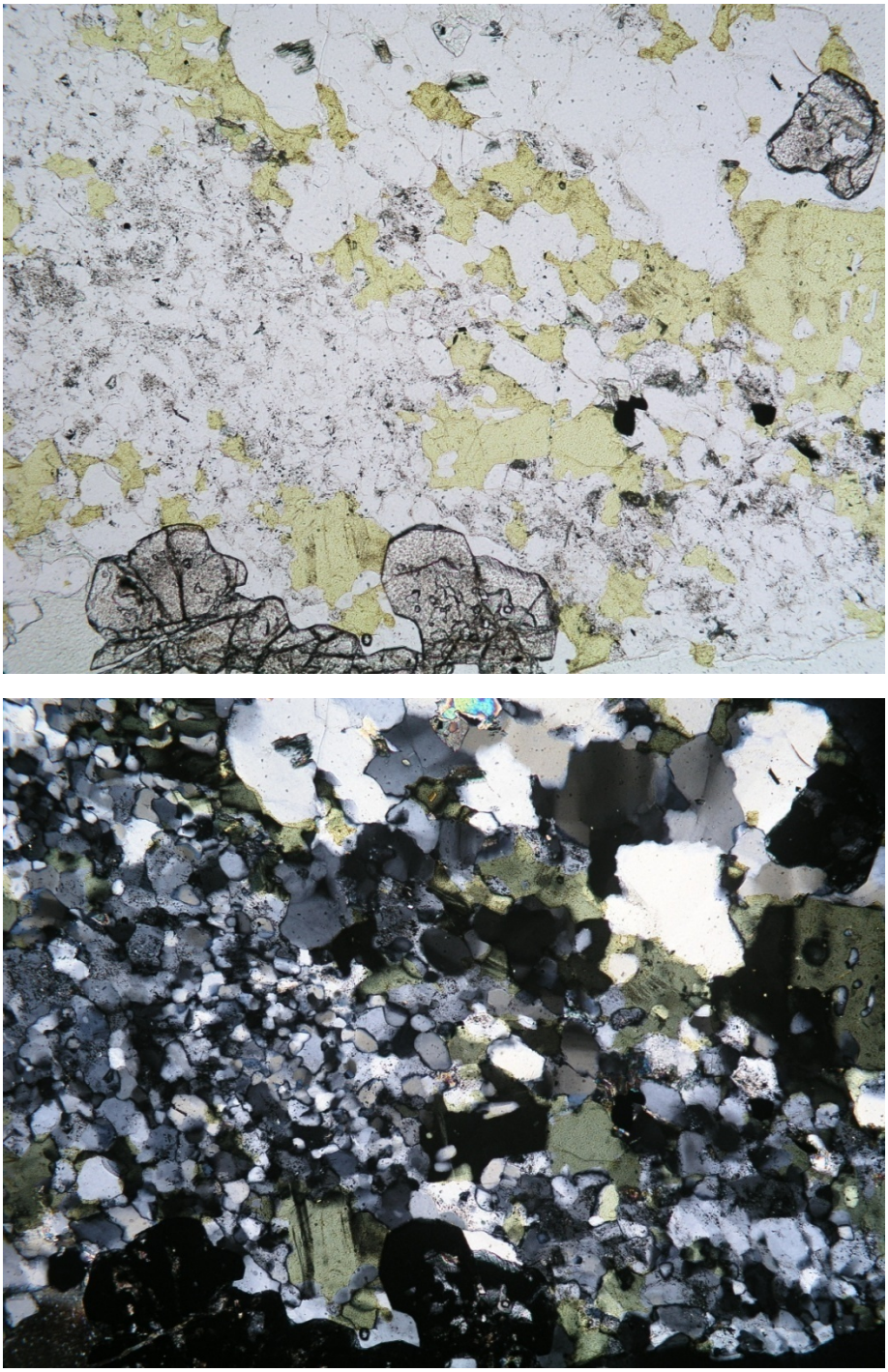

Fig. 2.13. Granite consisting of K-feldspar, quartz and plagioclase (colorless) and garnet (high relief crystals along bottom edge). Upper photomicrograph: plane polarized light; lower photomicrograph: crossed nicols. From 10090 ft in 33A-7 ST-1. Field of view is 1.6 mm across.

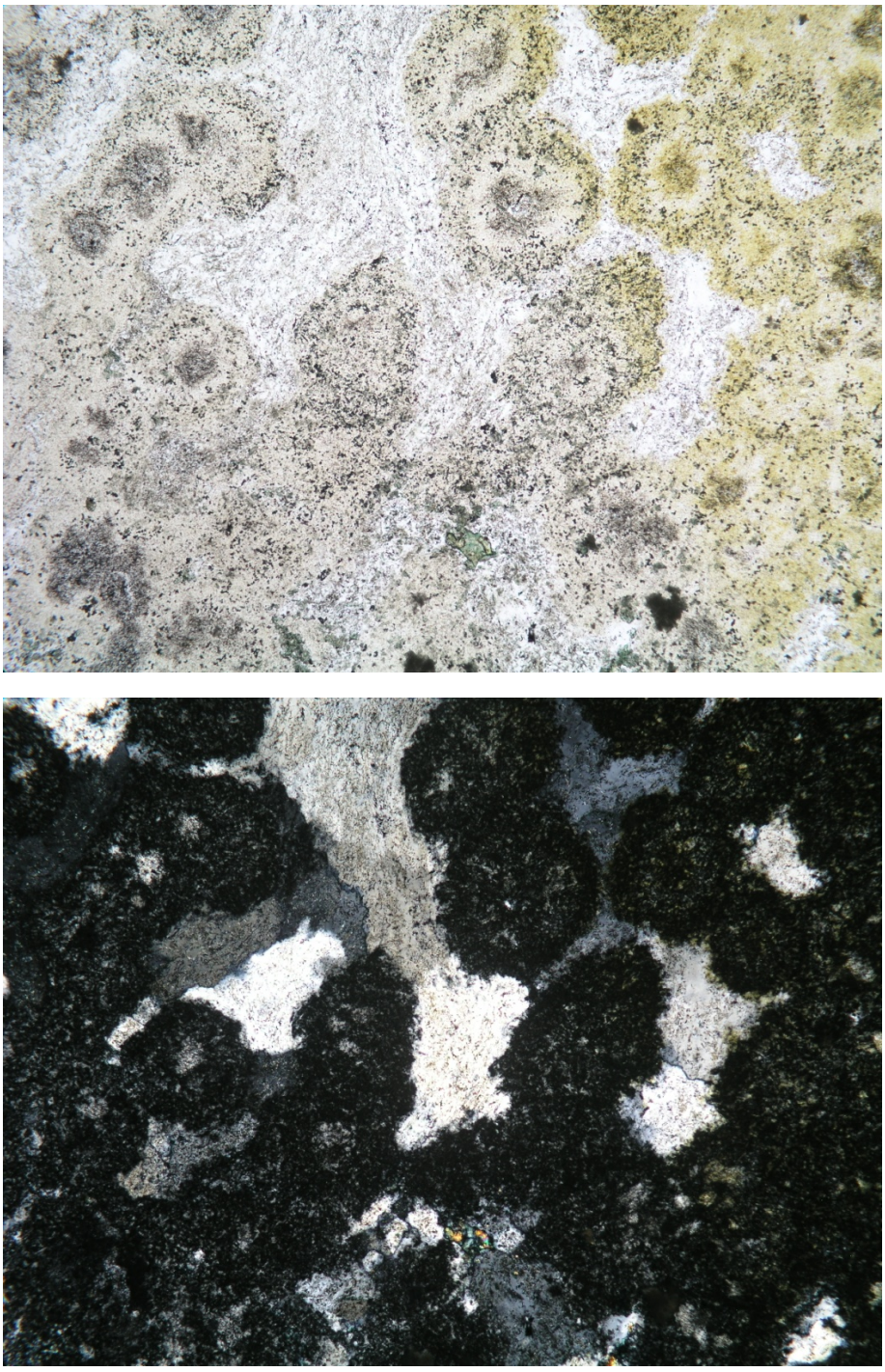

Fig. 2.14. Devitrified rhyolite containg spherulites of K-feldspar (right portion only stained yellow) and quartz in a in a quartz-rich matrix. Upper photomicrograph: plane polarized light; lower photomicrograph: crossed nicols. From 9300 ft in 33A-7 ST-1. Field of view is 0.8 mm across.

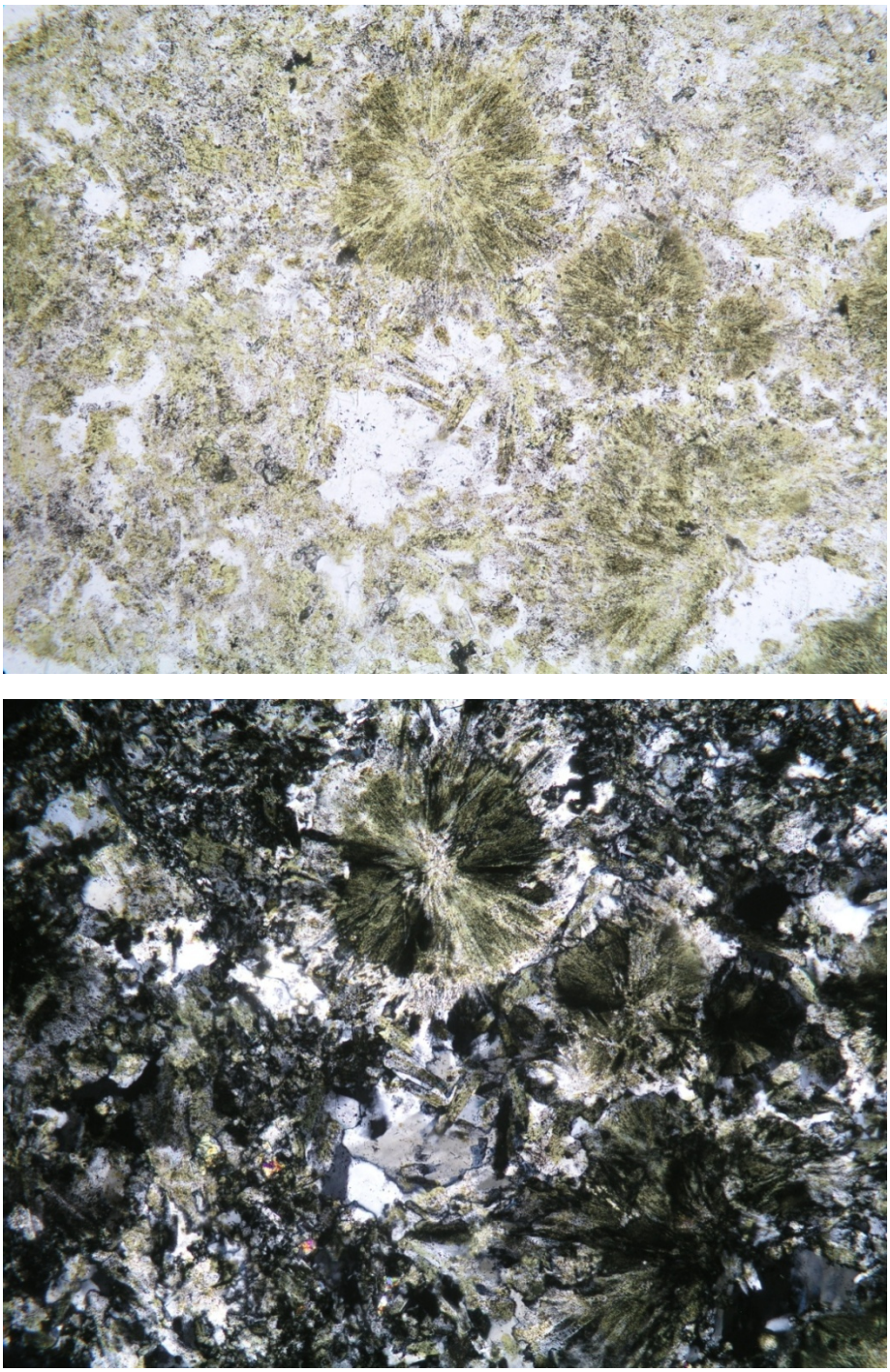

Fig. 2.15 Rhyolite containing spherulites of K-feldspar (stained yellow) and quartz in a quartz-rihc matrix. Upper photomicrograph: plane polarized light; lower photomicrograph: crossed nicols. From 9410 ft in 33A-7 ST-1. Field of view is 1.6 mm across.

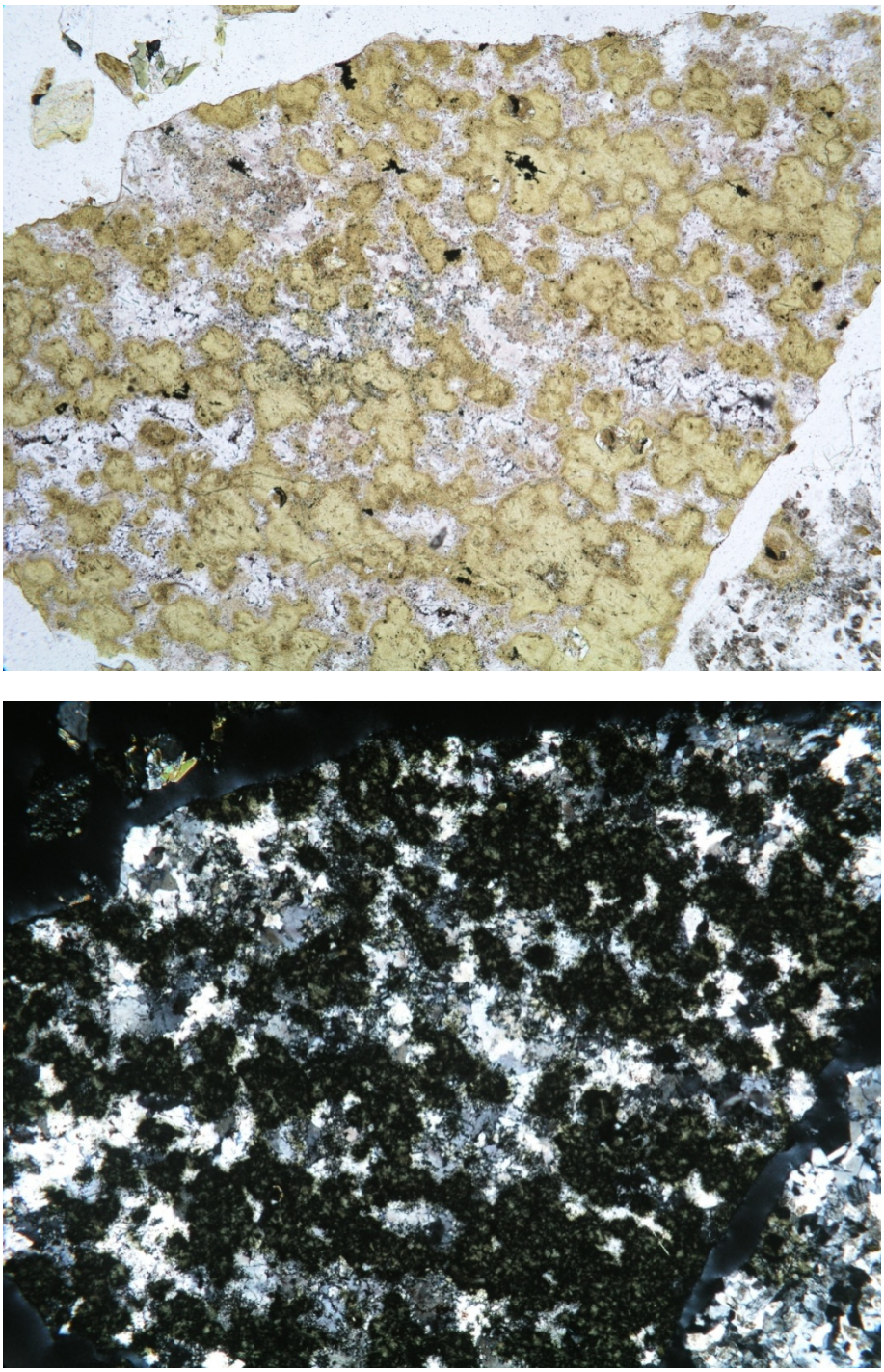

Fig. 2.16. Weakly silicified rhyolite containing K-feldspar rich (stained yellow) spherulites and quartz (colorless). Upper photomicrograph: plane polarized light; lower photomicrograph: crossed nicols. From 7680 ft in 33A-7. Field of view is 1.6 mm across.

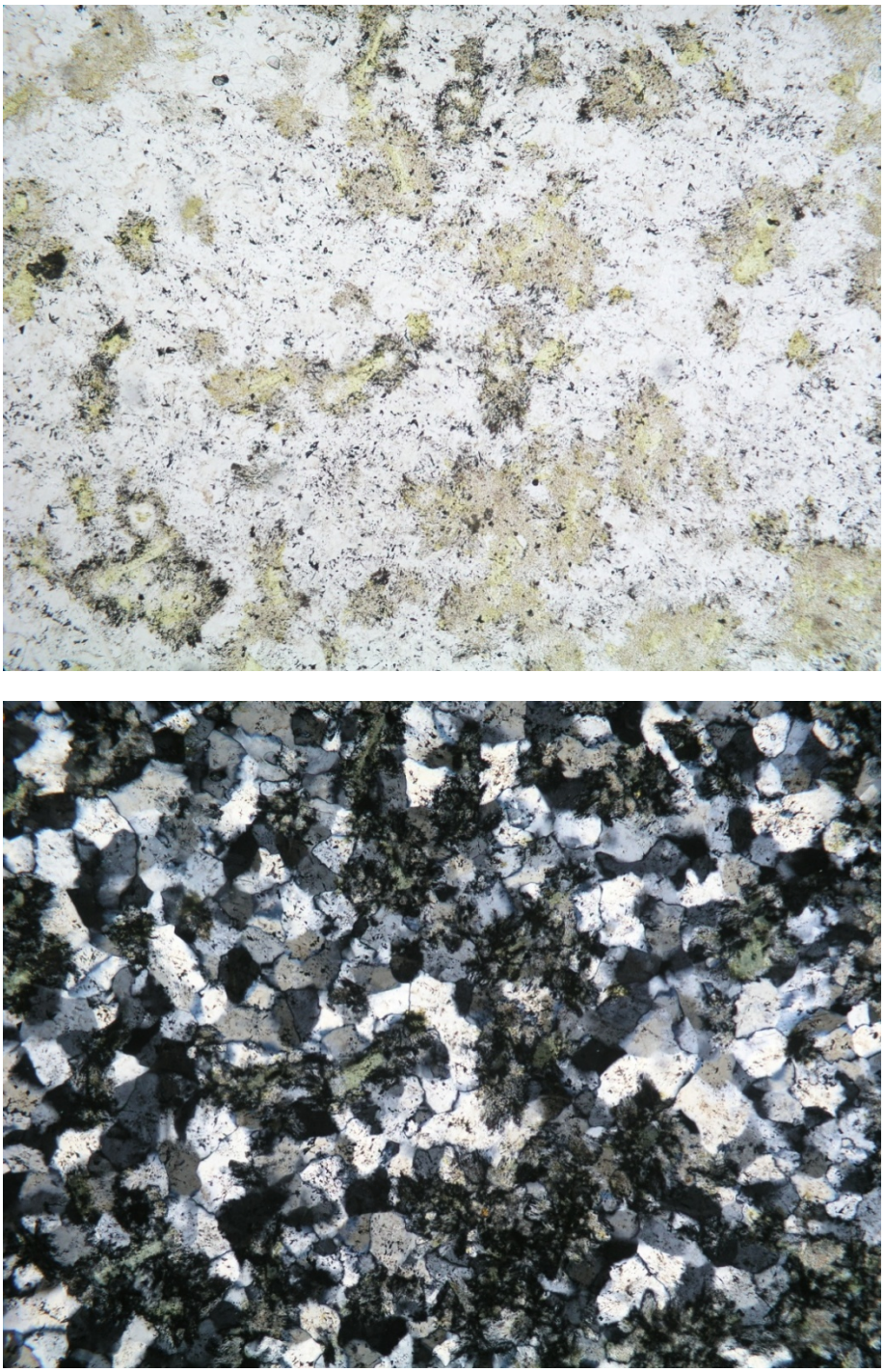

Fig. 2.17. Silicified rhyolite containing ghosts of K-feldspar rich (stained yellow) spherulites in a matrix of quartz. Upper photomicrograph: plane polarized light; lower photomicrograph: crossed nicols. From 7680 ft in 33A-7. Field of view is 0.8 mm across.

33A-7 Veins

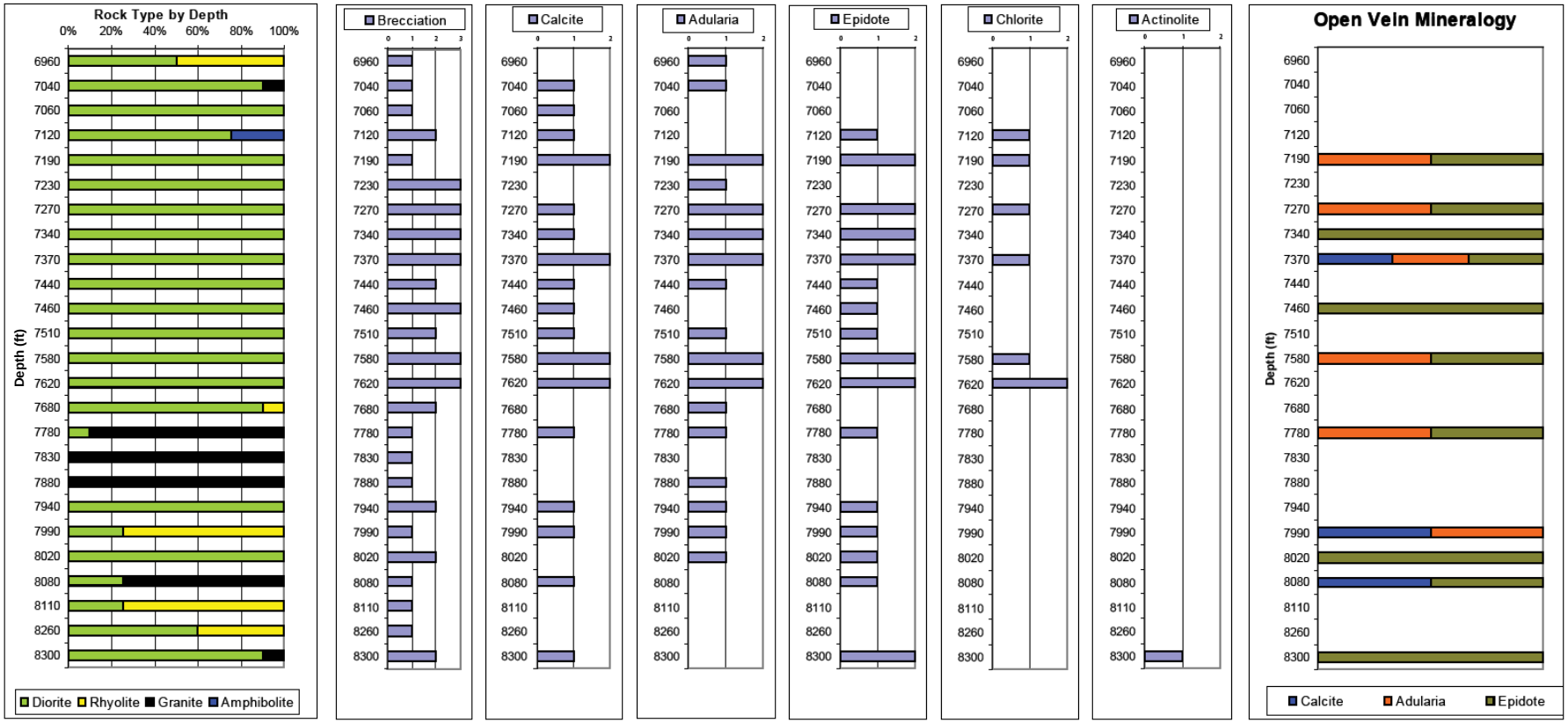

Fig. 3.1. Distribution of rock types, tectonic breccias, vein minerals and open (porous) veins in 33A-7.

33A-7 ST-1 Veins

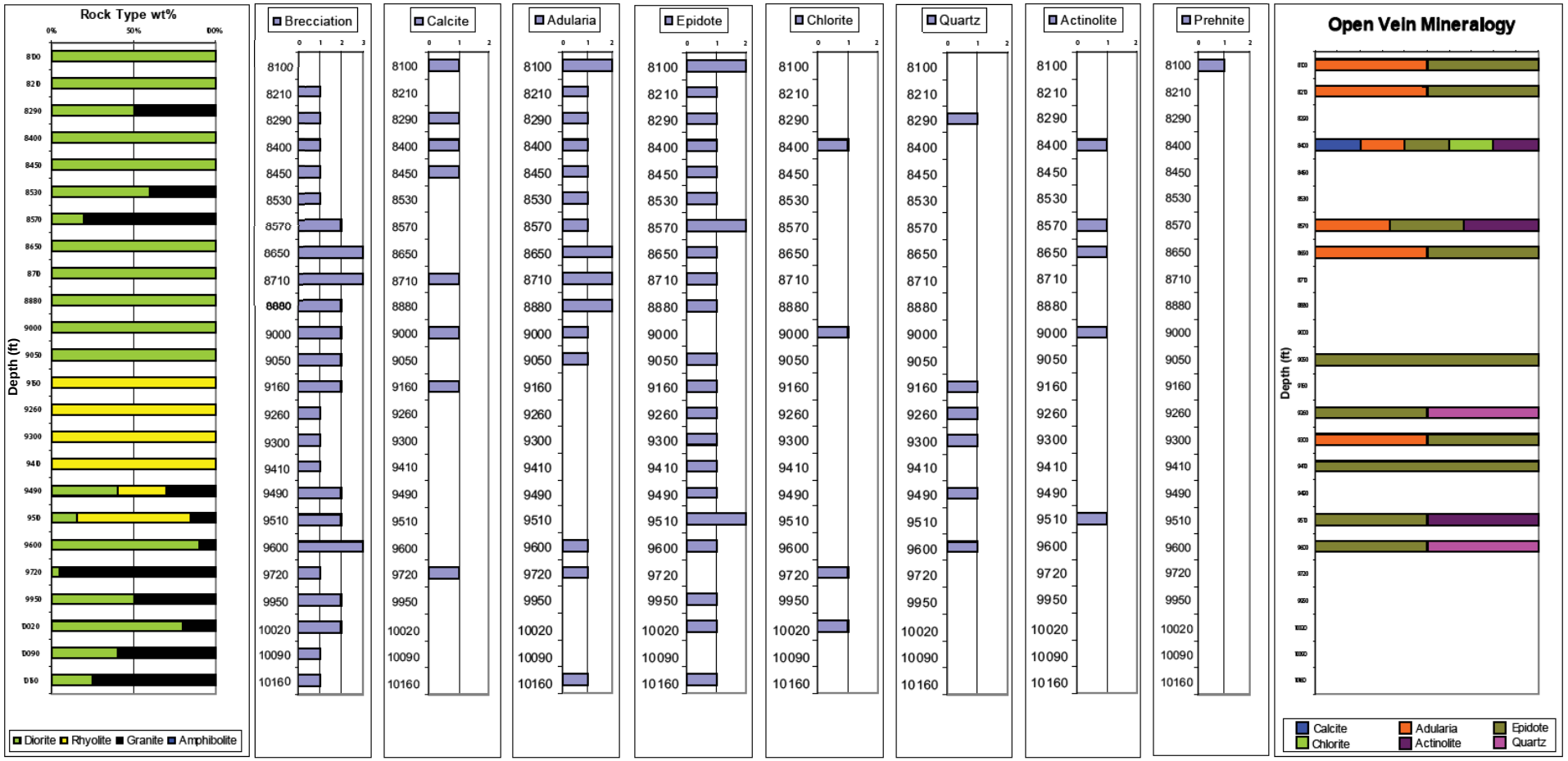

Fig. 3.2. Distribution of rock types, tectonic breccias, vein minerals and open (porous) veins in 33A-7 ST-1.

83-11 Veins

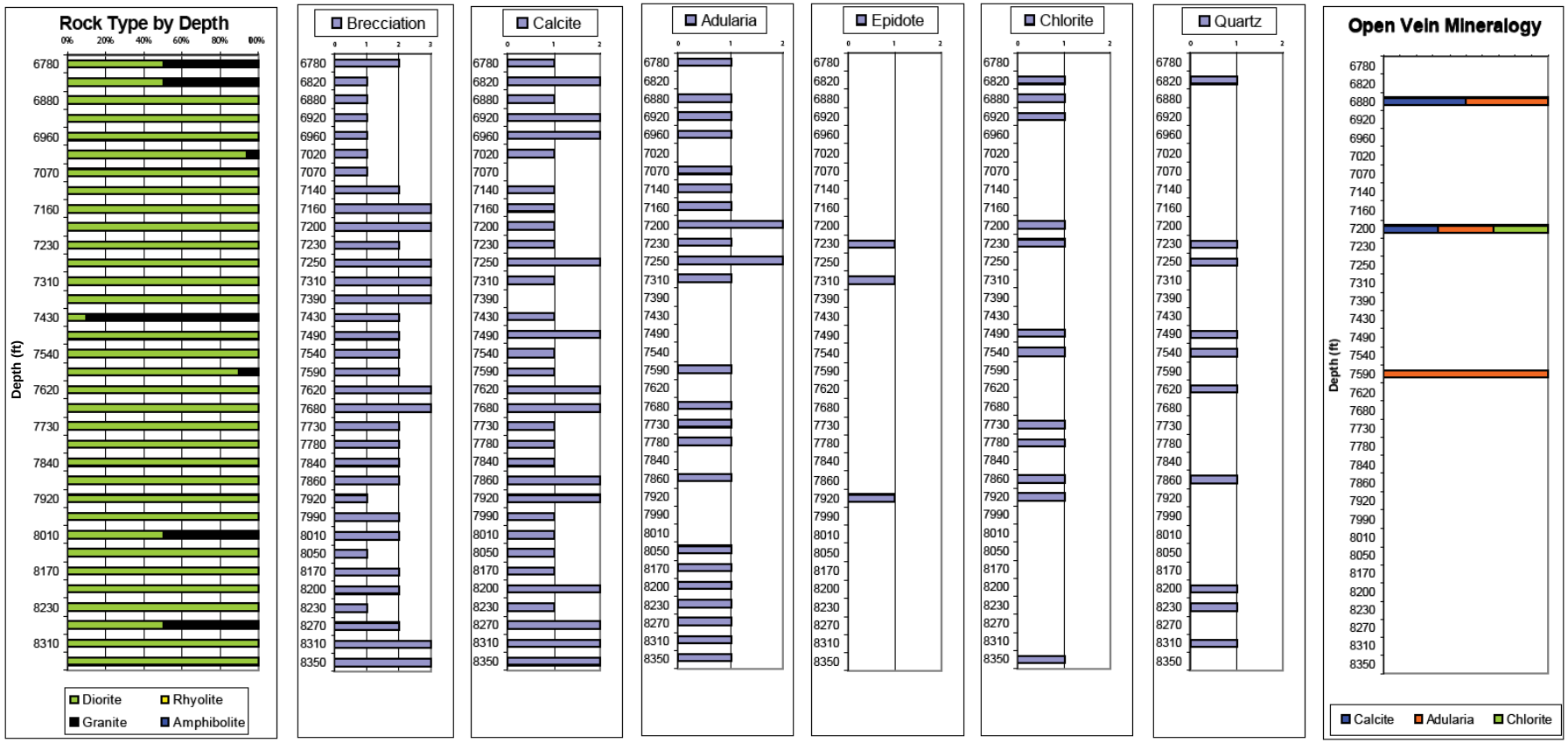

Fig.-3.3. Distribution of rock types, tectonic breccias, vein minerals and open (porous) veins in 83-11.

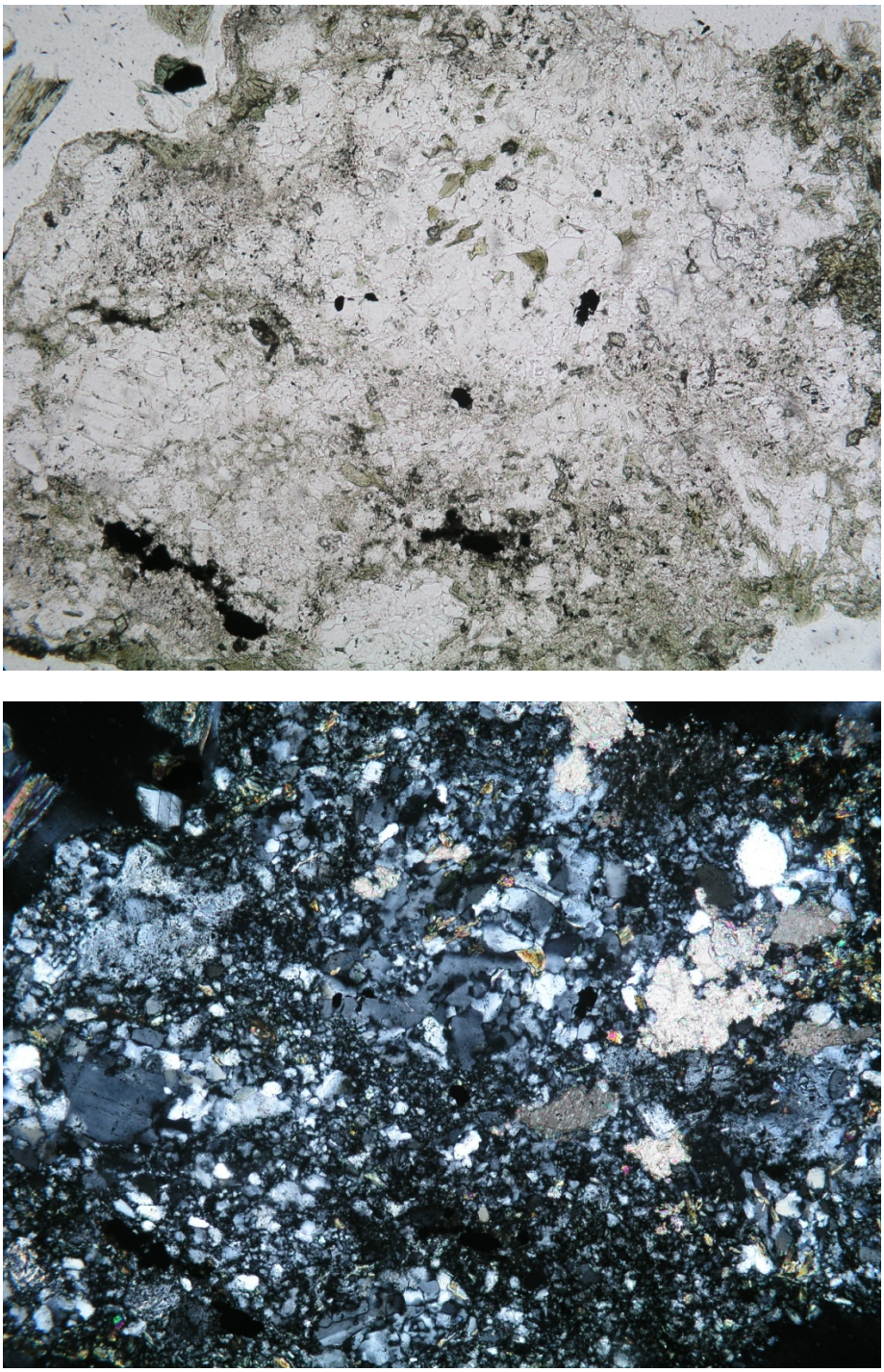

Fig. 3.4. Brecciated granite. Upper photomicrograph: plane polarized light; lower photomicrograph: crossed nicols. From 8310 ft in 83-11. Field of view is 3.1 mm across.

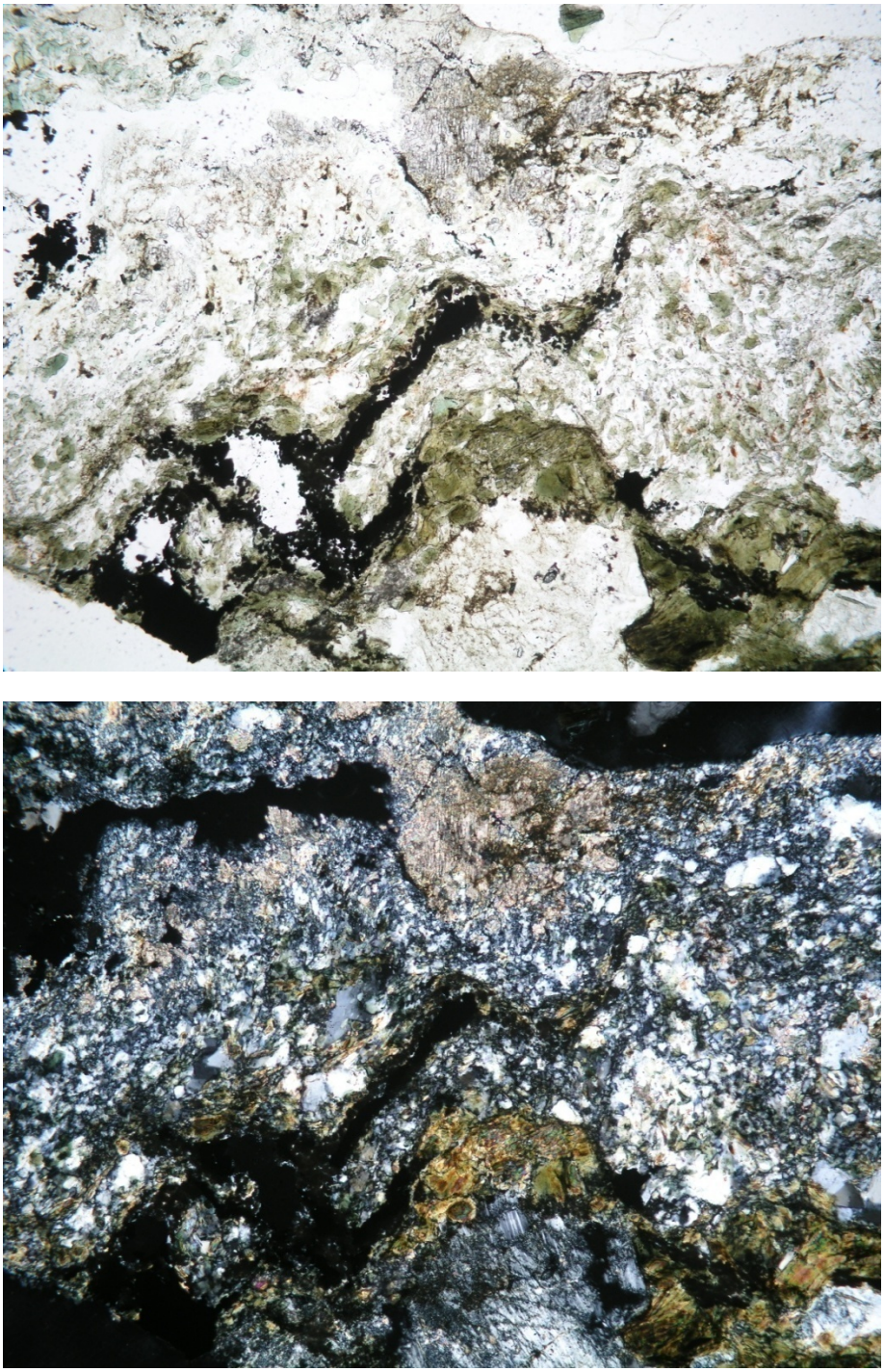

Fig. 3.5. Brecciated diorite partially altered to calcite (colorless with high-relief, top center). Hornblende (green) on lower edge is fresh. Chlorite (light green) forms small grains within the finely ground diorite in the center of the image. Upper photomicrograph: plane polarized light; lower photomicrograph: crossed nicols. From 7250 ft in 83-11. Field of view is 3.1 mm across.

Fig. 3.6. Sheared diorite cut by veins of epidote (northwest–trending veins; colorless to pale green, high-relief), and later calcite (northeast-trending veins; upper right corner of chip) veins. The veins are not sheared and thus must postdate the tectonic activity. Upper photomicrograph plane polarized light, lower photomicrograph crossed nicols. From 7310 ft in 83-11. Field of view is 3.1 mm across.

33A-7 Mineralogy

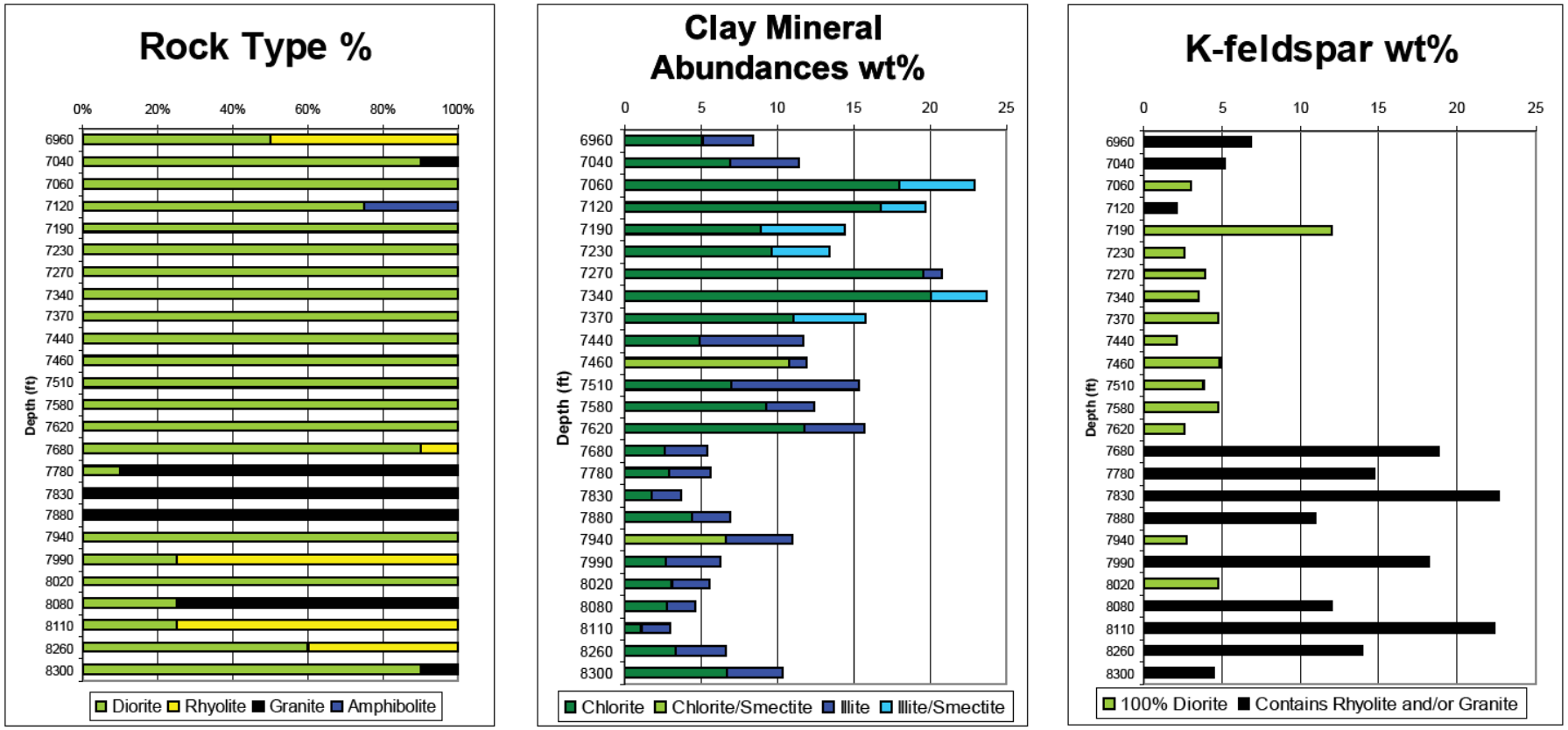

Fig.-3.7. Distribution of rock types, clay alteration and potassium feldspar 33A-7.

33A-7 ST-1Mineralogy

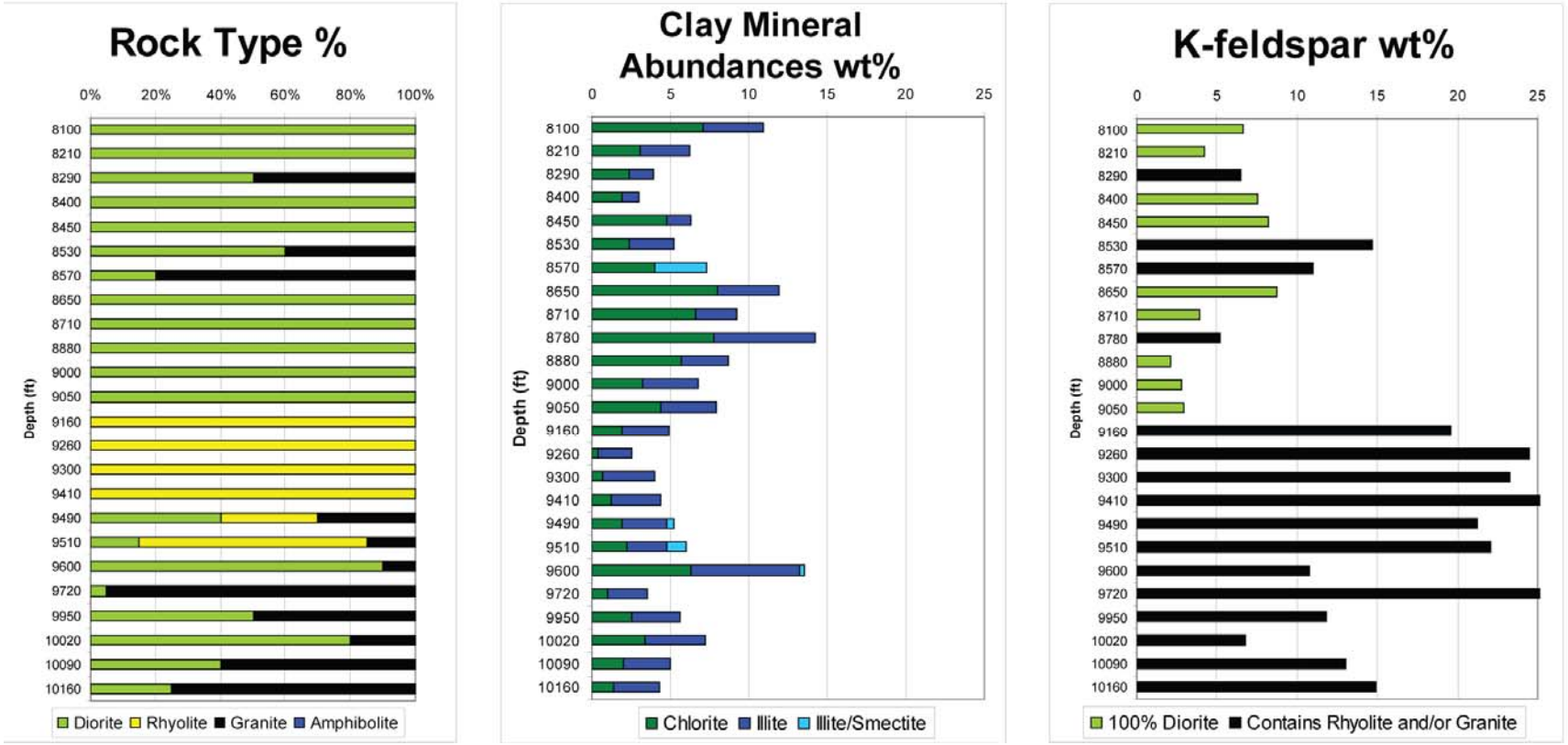

Fig.-3.8. Distribution of rock types, clay alteration and potassium feldspar 33A-7 ST-1.

83-11 Mineralogy

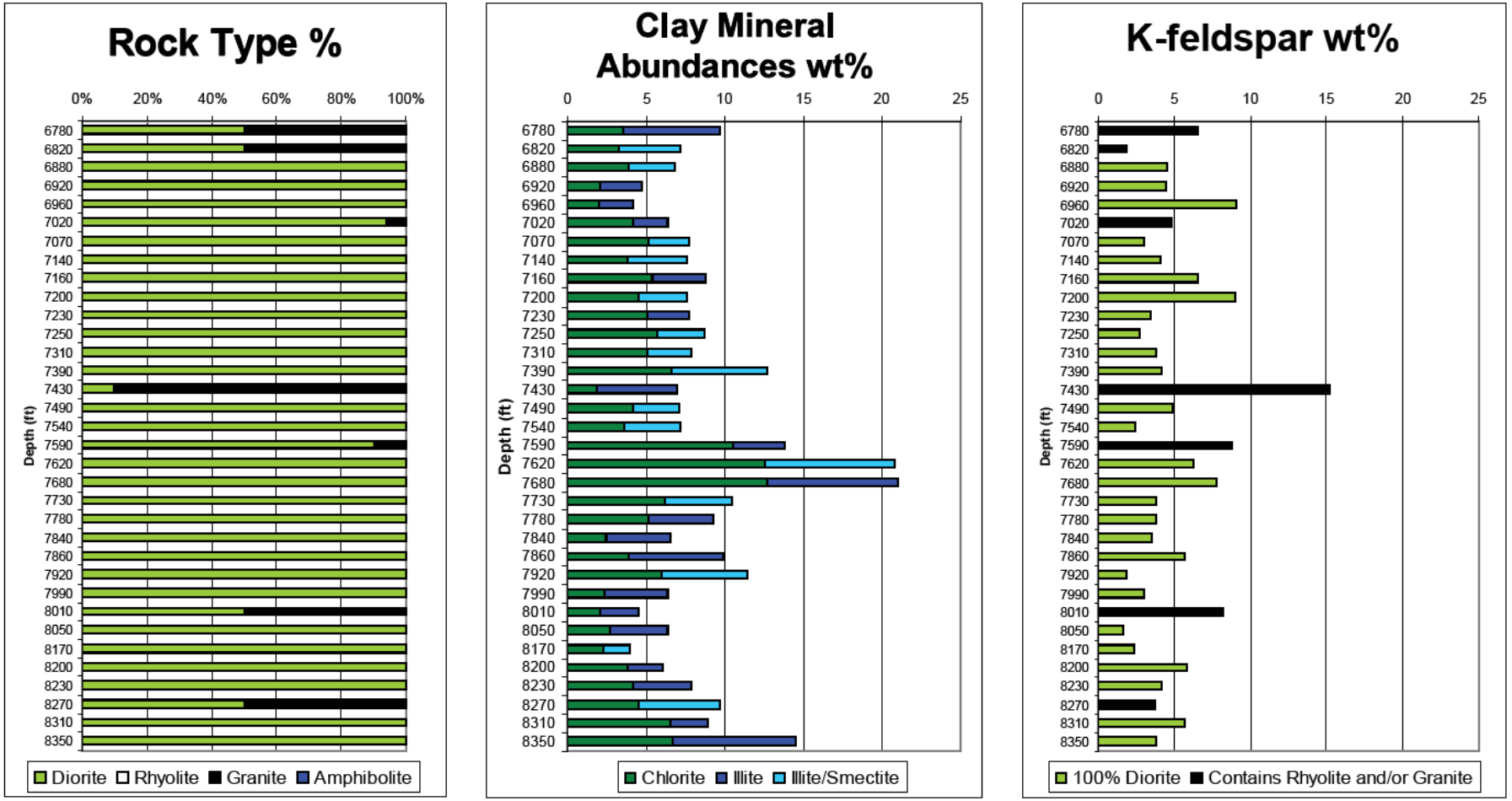

Fig.-3.9. Distribution of rock types, clay alteration and potassium feldspar in 83-11.

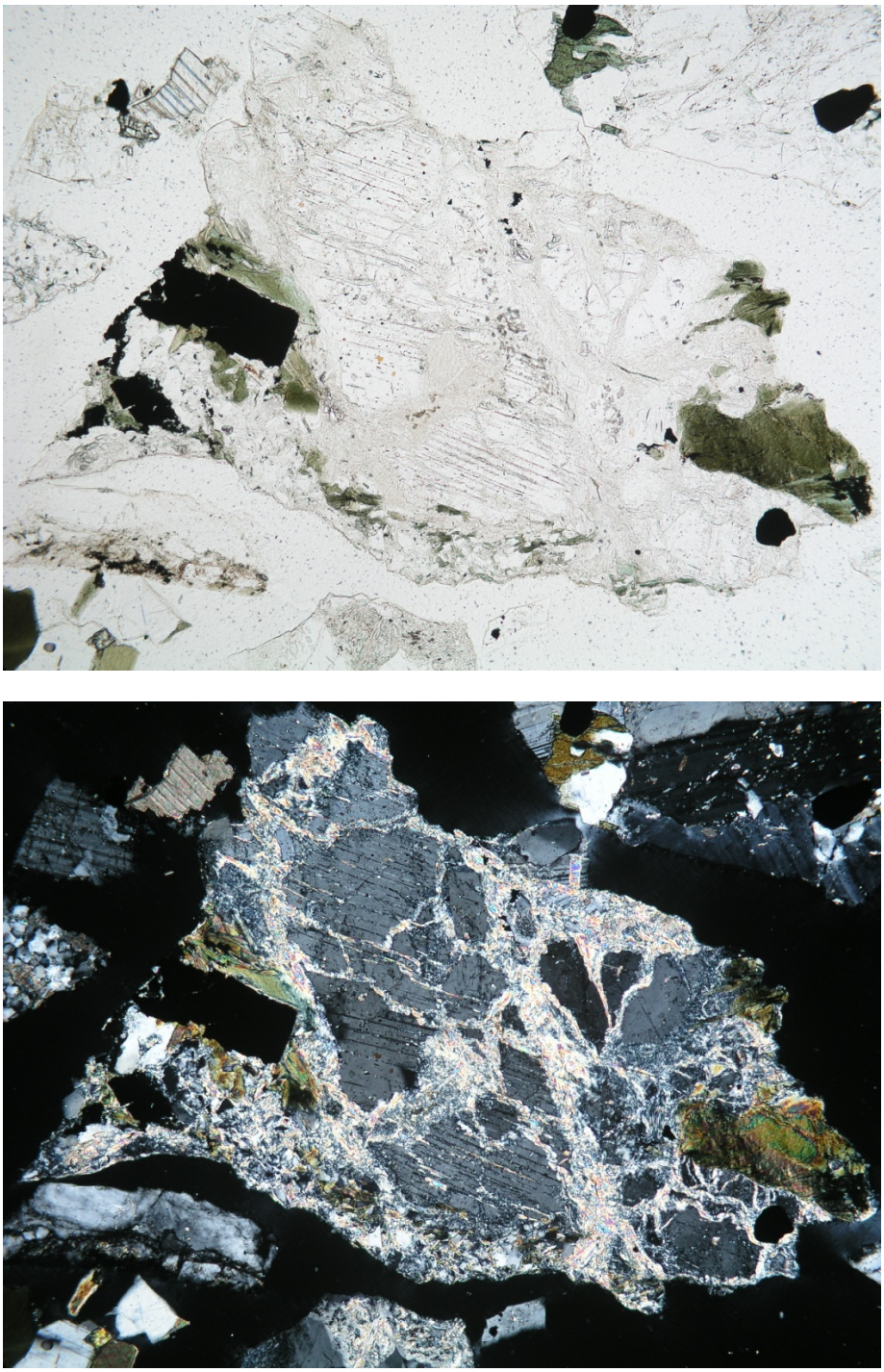

Fig. 3.10. Plagioclase replaced by illite along fractures in brecciated diorite. Upper photomicrograph: plane polarized light; lower photomicrograph: crossed nicols. From 7020 ft in 83-11. Field of view is 3.1 mm across.

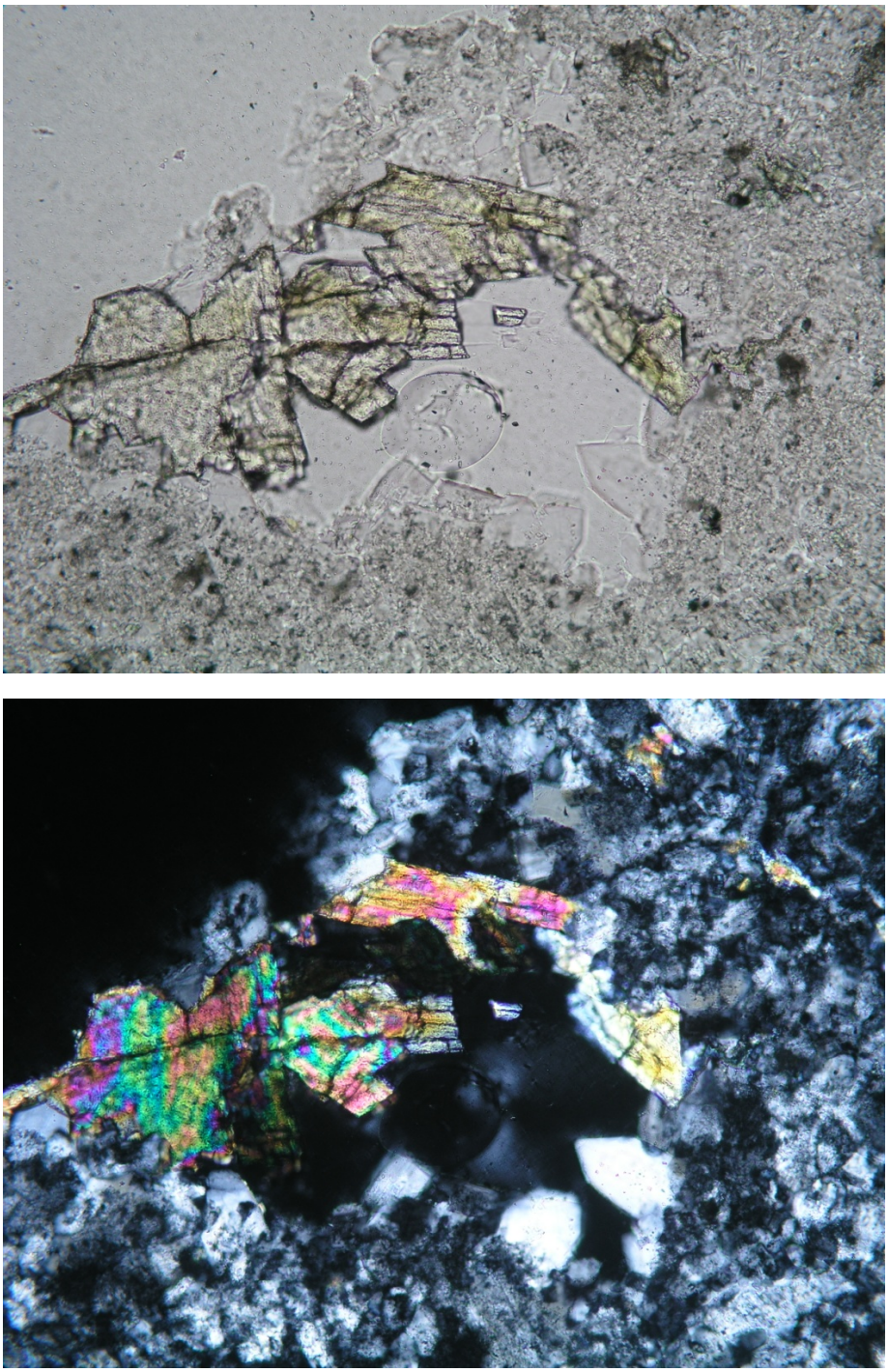

Fig. 3.11. Quartz (colorless) and epidote (colorless to yellow-green, high relief) filling a vug in devitrified rhyolite. Upper photomicrograph: plane polarized light; lower photomicrograph: crossed nicols. From 9260 ft in 33A-7 ST-1. Field of view is 0.8 mm across.

Fig. 3.12. Epidote vein in devitrified rhyolite. Upper photomicrograph: plane polarized light; lower photomicrograph: crossed nicols. From 7990 ft in 33A-7. Field of view is 1.6 mm across.

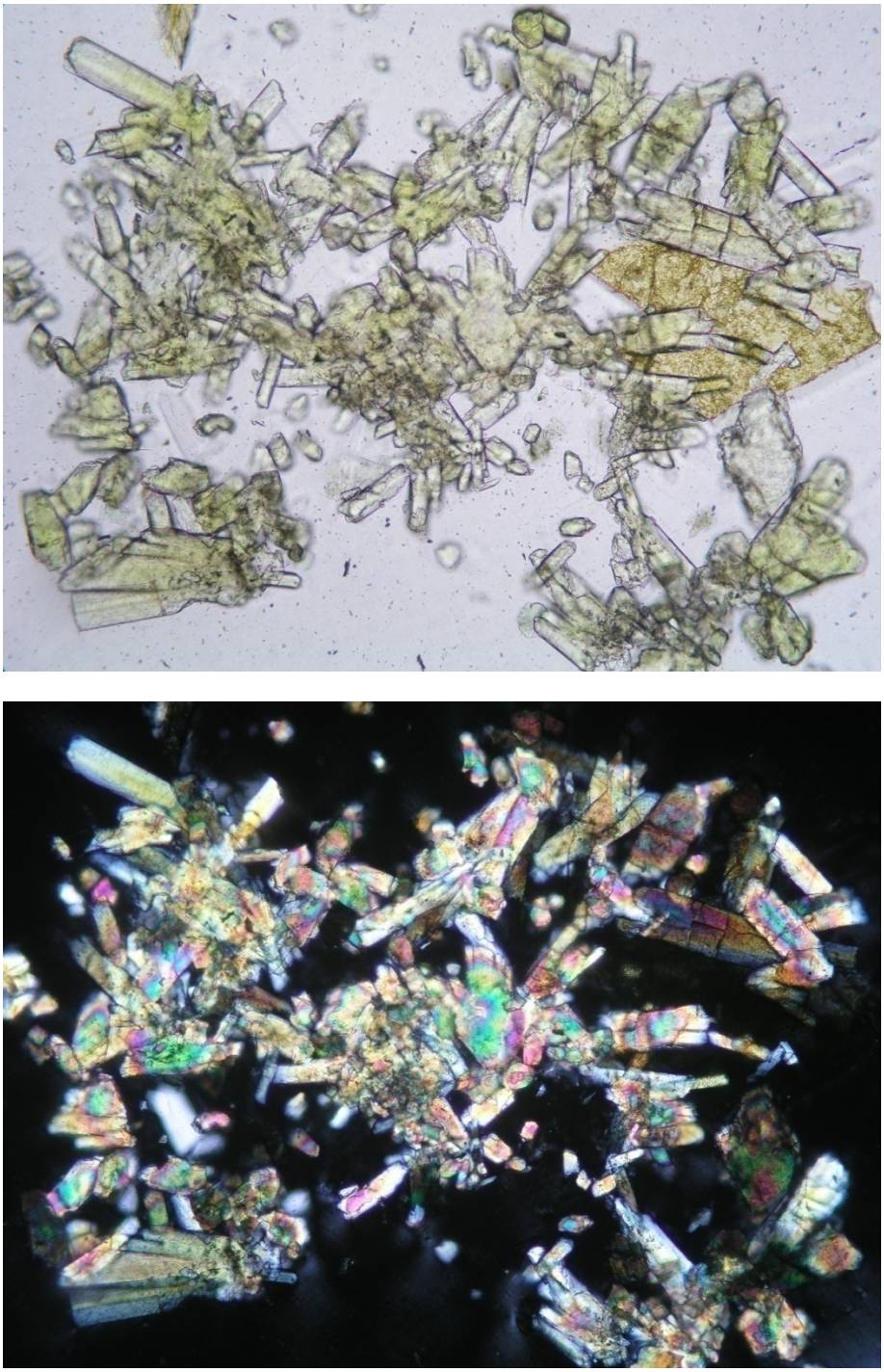

Fig. 3.13. Vein consisting of euhedral epidote crystals and rhombic crystals of adularia (stained yellow, right side of image). Upper photomicrograph: plane polarized light; lower photomicrograph: crossed nicols. From 7780 ft in 33A-7. Field of view is 0.8 mm across.

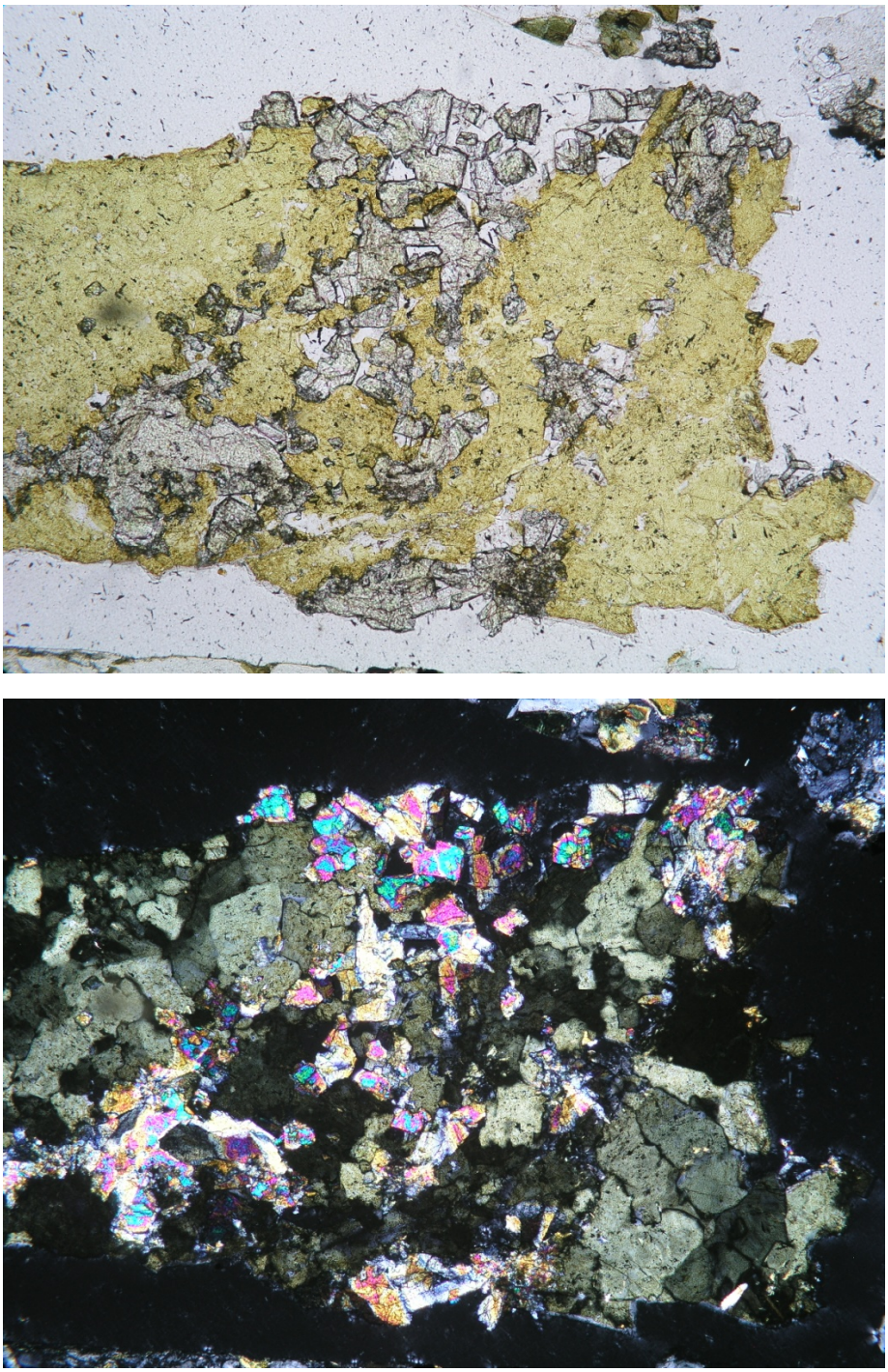

Fig. 3.14. Open vein of epidote (colorless to yellow-green, high relief) and later adularia (stained yellow). Upper photomicrograph: plane polarized light; lower photomicrograph: crossed nicols. From 8650 ft in 33A-7 ST-1. Field of view is 1.6 mm across.

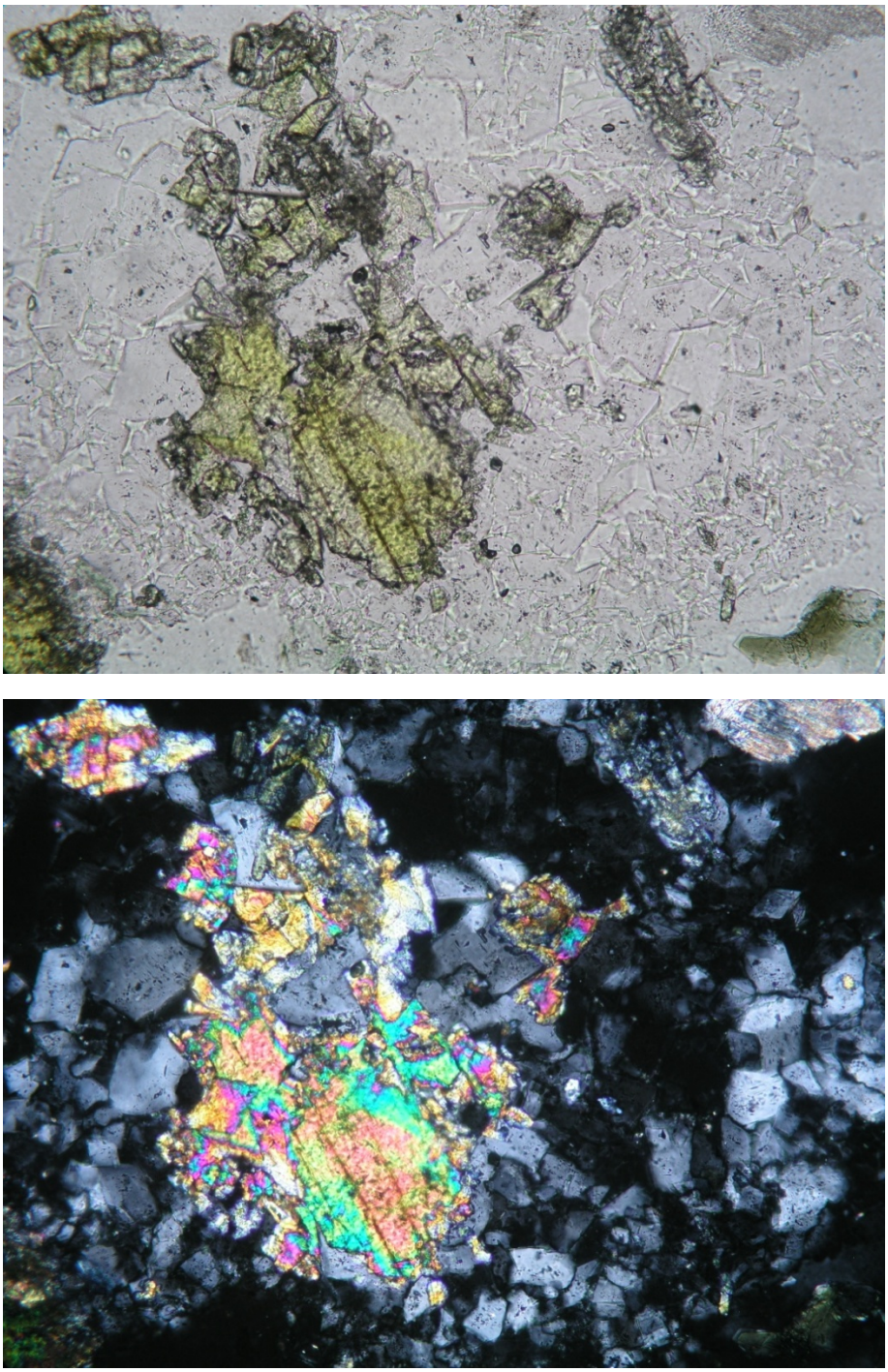

Fig. 3.15. Open vein of adularia (not stained) and epidote. From 7580 ft in 33A-7. Upper photomicrograph: plane polarized light; lower photomicrograph: crossed nicols. Field of view is 1.6 mm across.

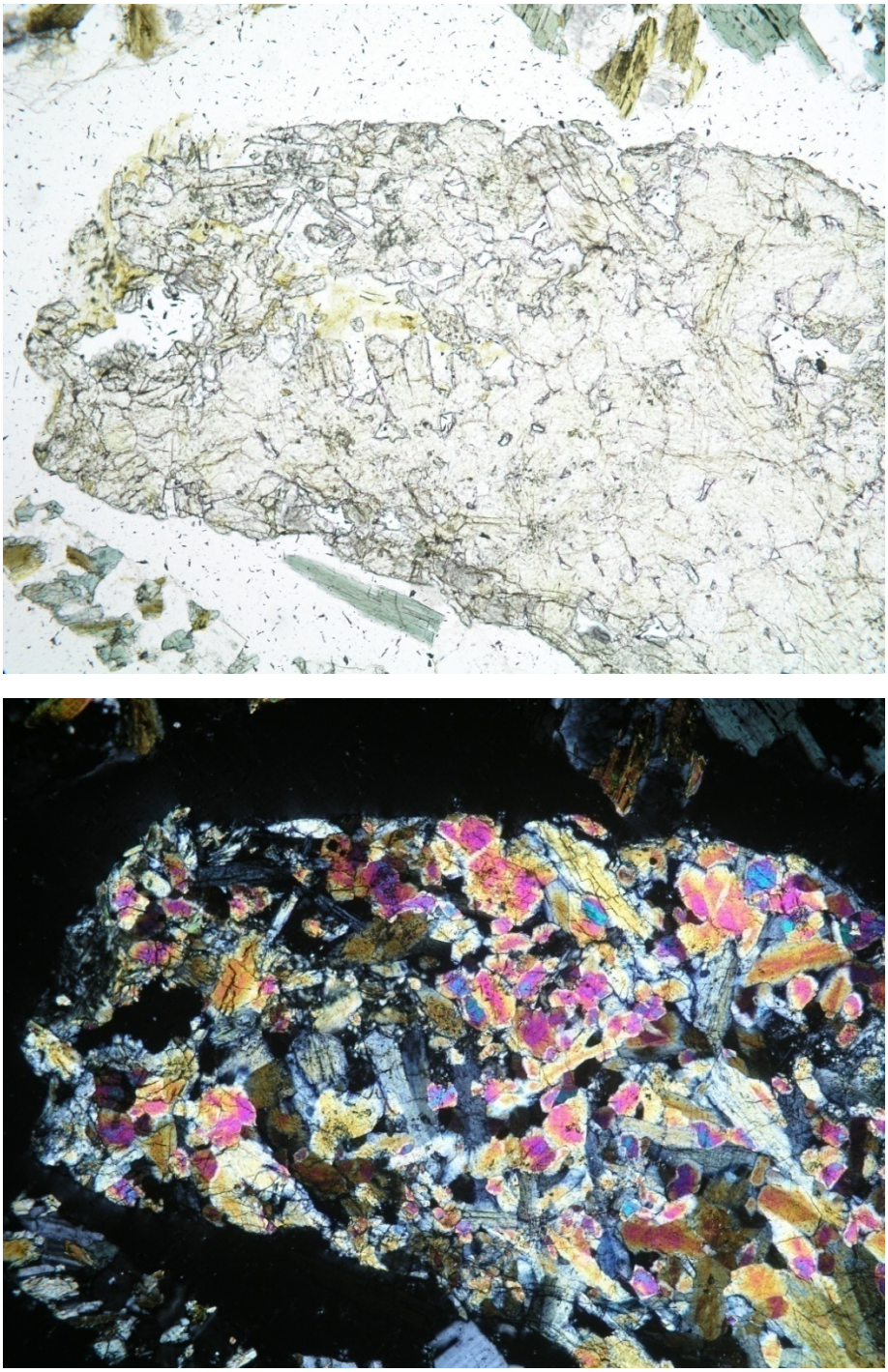

Fig. 3.16. Open vein consisting primarily of epidote (colorless to yellow-green, high relief). Traces of adularia (stained yellow) and illite (not visible in image) were also deposited in the vein. From 9000 ft in 33A-7 ST-1. Upper photomicrograph: plane polarized light; lower photomicrograph: crossed nicols. Field of view is 1.6 mm across.

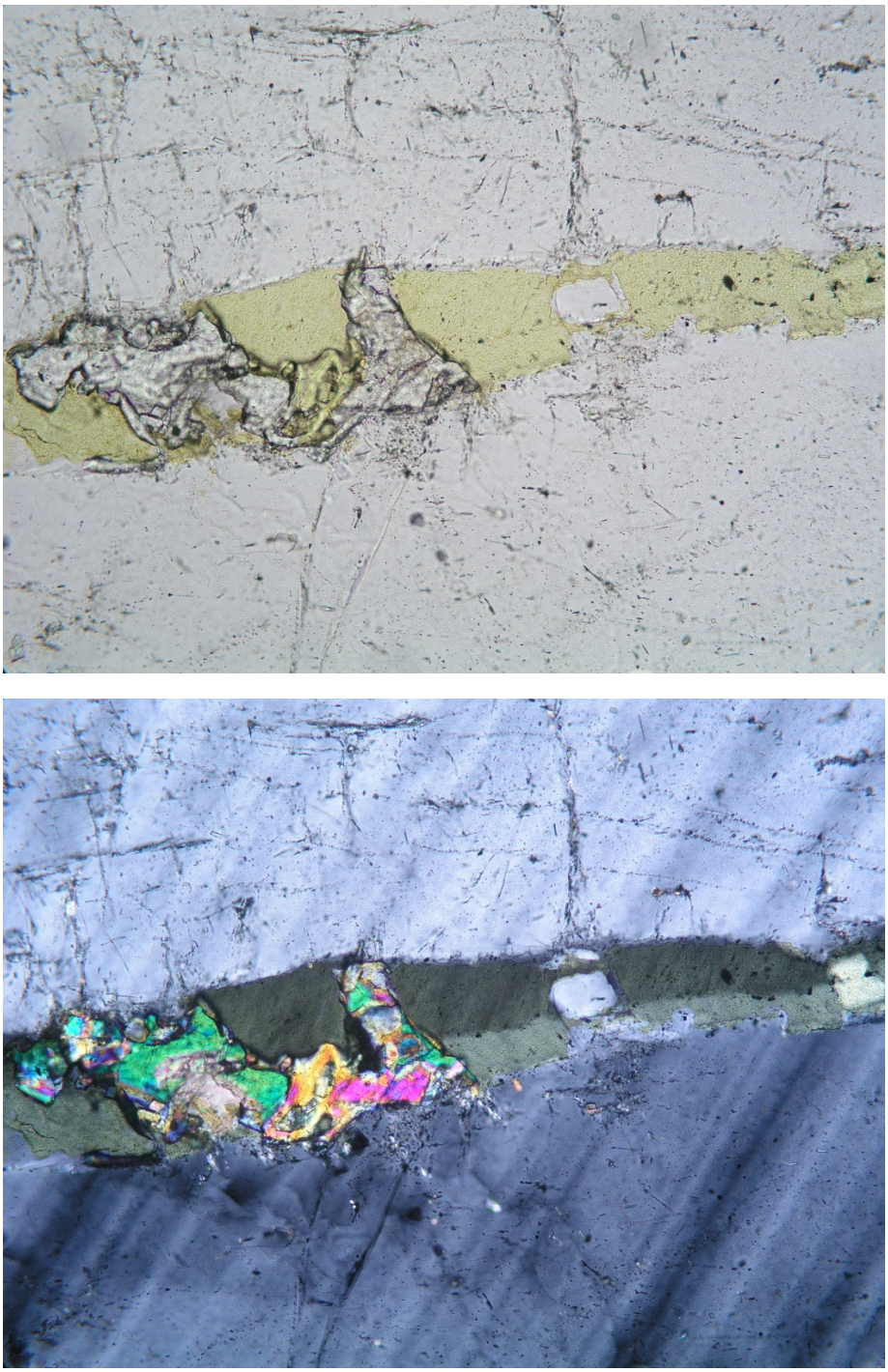

Fig. 3.17. Vein containing epidote (colorless to yellow-green, high relief) and later adularia (stained yellow). From 8530 ft in 33A-7 ST-1. Upper photomicrograph: plane polarized light; lower photomicrograph: crossed nicols. Field of view is 0.8 mm across.

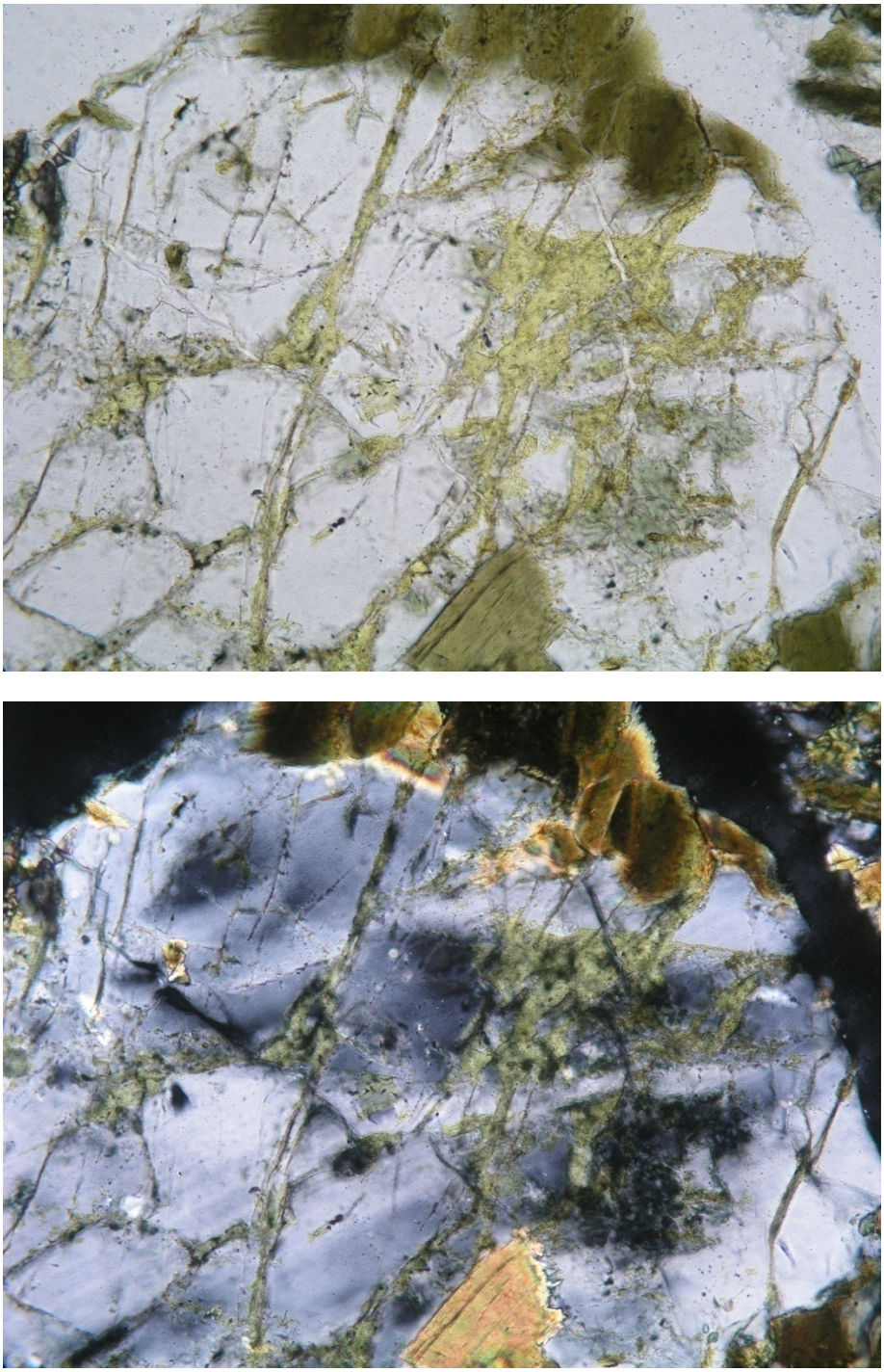

Fig. 3.18. Plagioclase in diorite veined and replaced by adularia (stained yellow) along fractures. Also visible are brown biotite crystals. Upper photomicrograph: plane polarized light; lower photomicrograph: crossed nicols. From 7140 ft in 83-11. Field of view is 1.6 mm across.

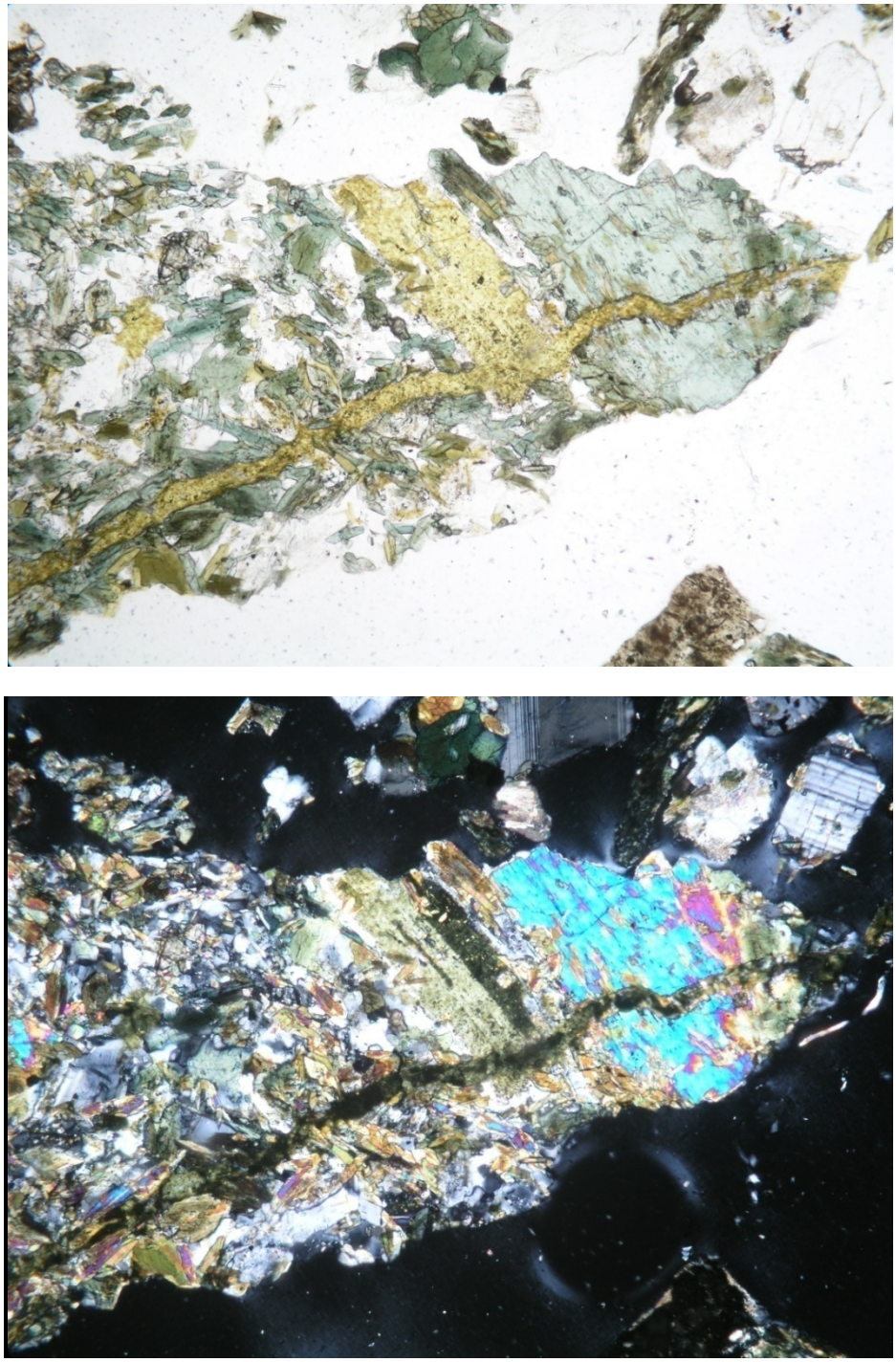

Fig. 3.19. Diorite cut by an adularia vein (stained yellow). The plagioclase phenocryst left of the vein was replaced by adularia. Upper photomicrograph: plane polarized light; lower photomicrograph: crossed nicols. From 7040 ft in 33A-7. Field of view is 3.1 mm across.

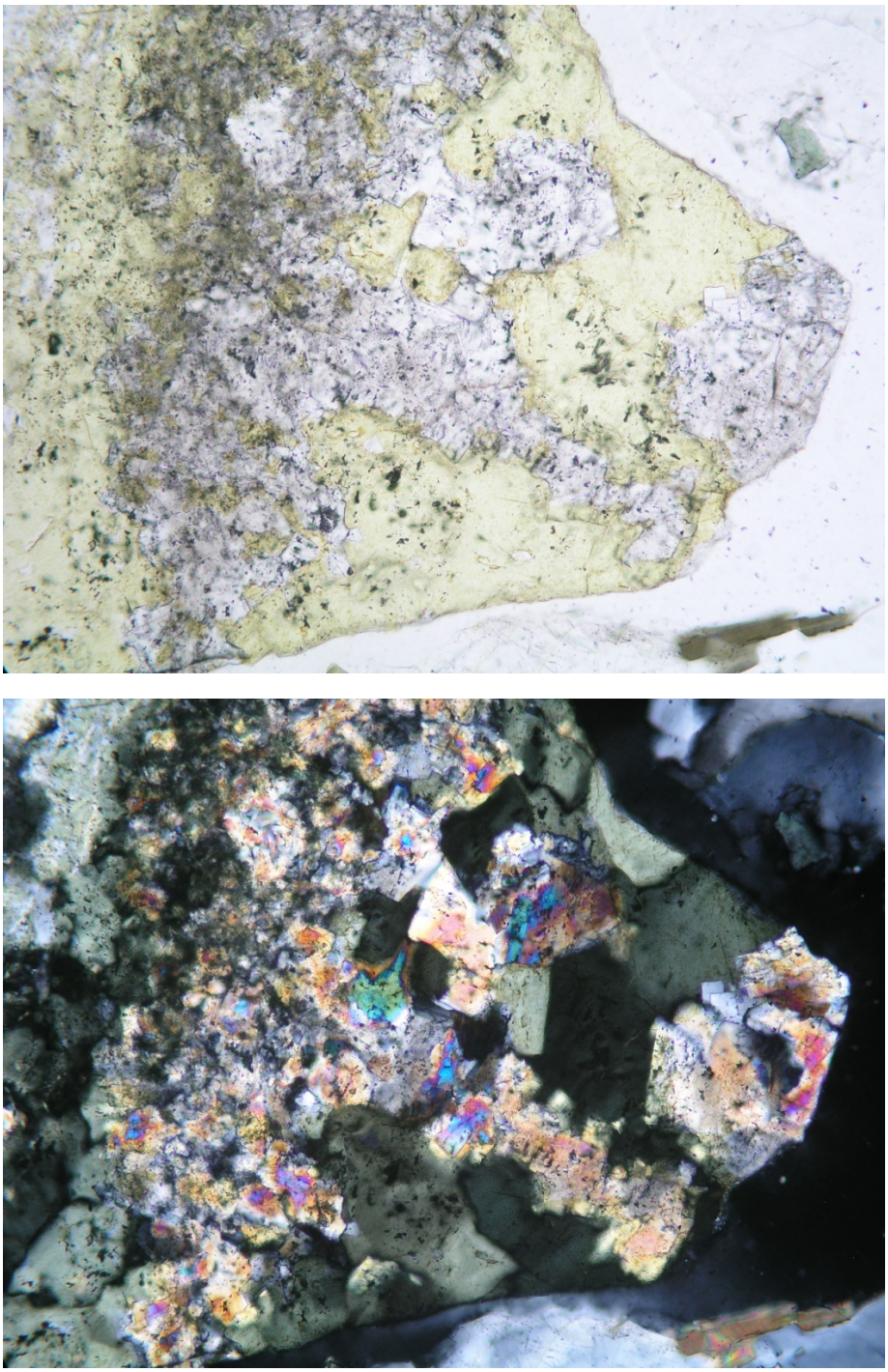

Fig. 3.20 Vein of adularia (stained yellow) and prehnite (brightly colored in lower image). Upper photomicrograph: plane polarized light; lower photomicrograph crossed nicols. From 8100 ft in 33A-7 ST-1. Field of view is 1.6 mm across.

Fig 3.21. Quatz vein cutting granite porphyry. From 8080 ft in 33A-7. Upper photomicrograph: plane polarized light; lower photomicrograph: crossed nicols. Field of view is 1.6 mm across.

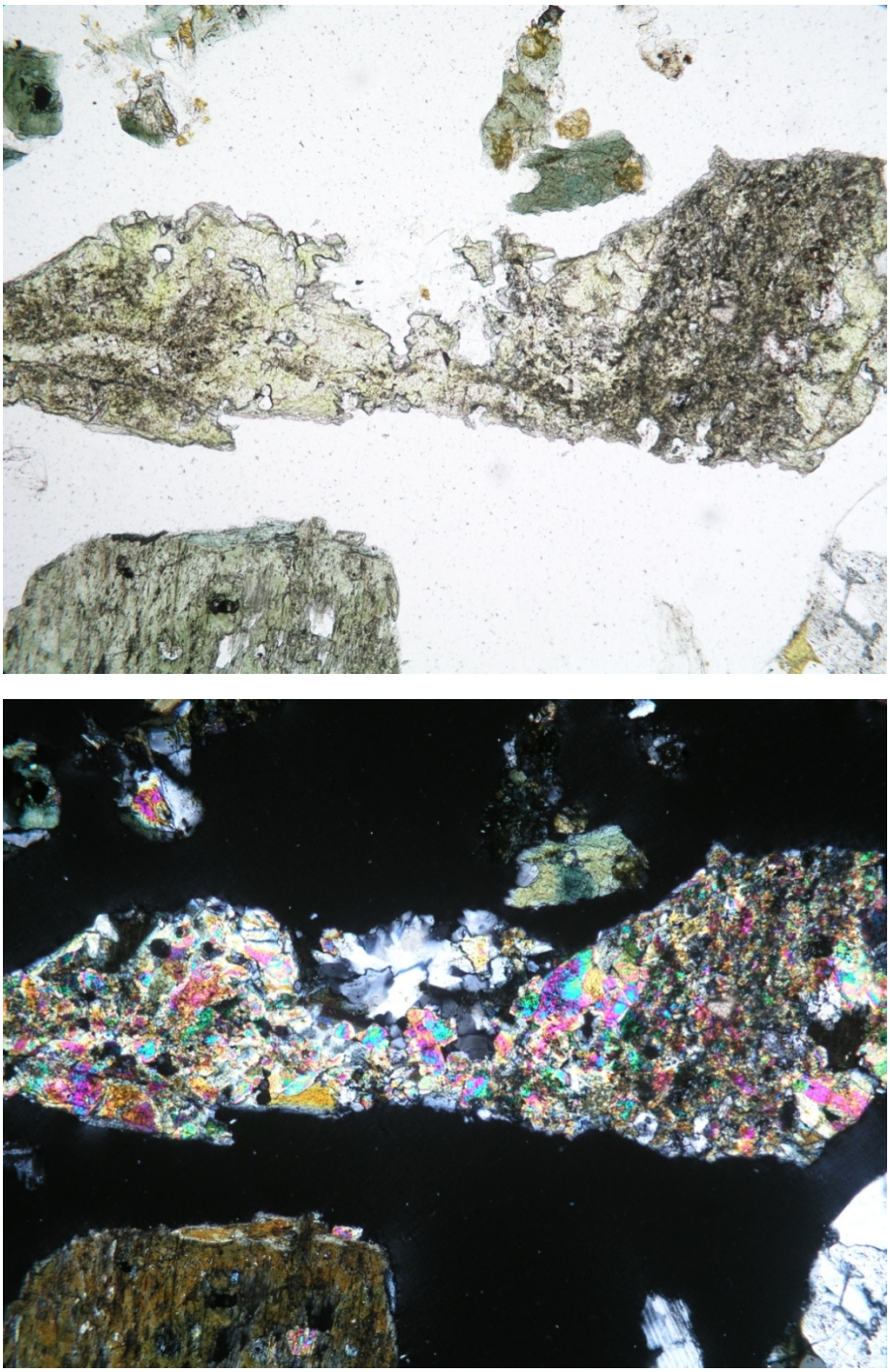

Fig. 3.22. Epidote (colorless to yellow-green, high relief) - quartz vein. Upper photomicrograph: plane polarized light; lower photomicrograph: crossed nicols. From 9600 ft in 33A-7 ST-1. Field of view is 1.6 mm across.

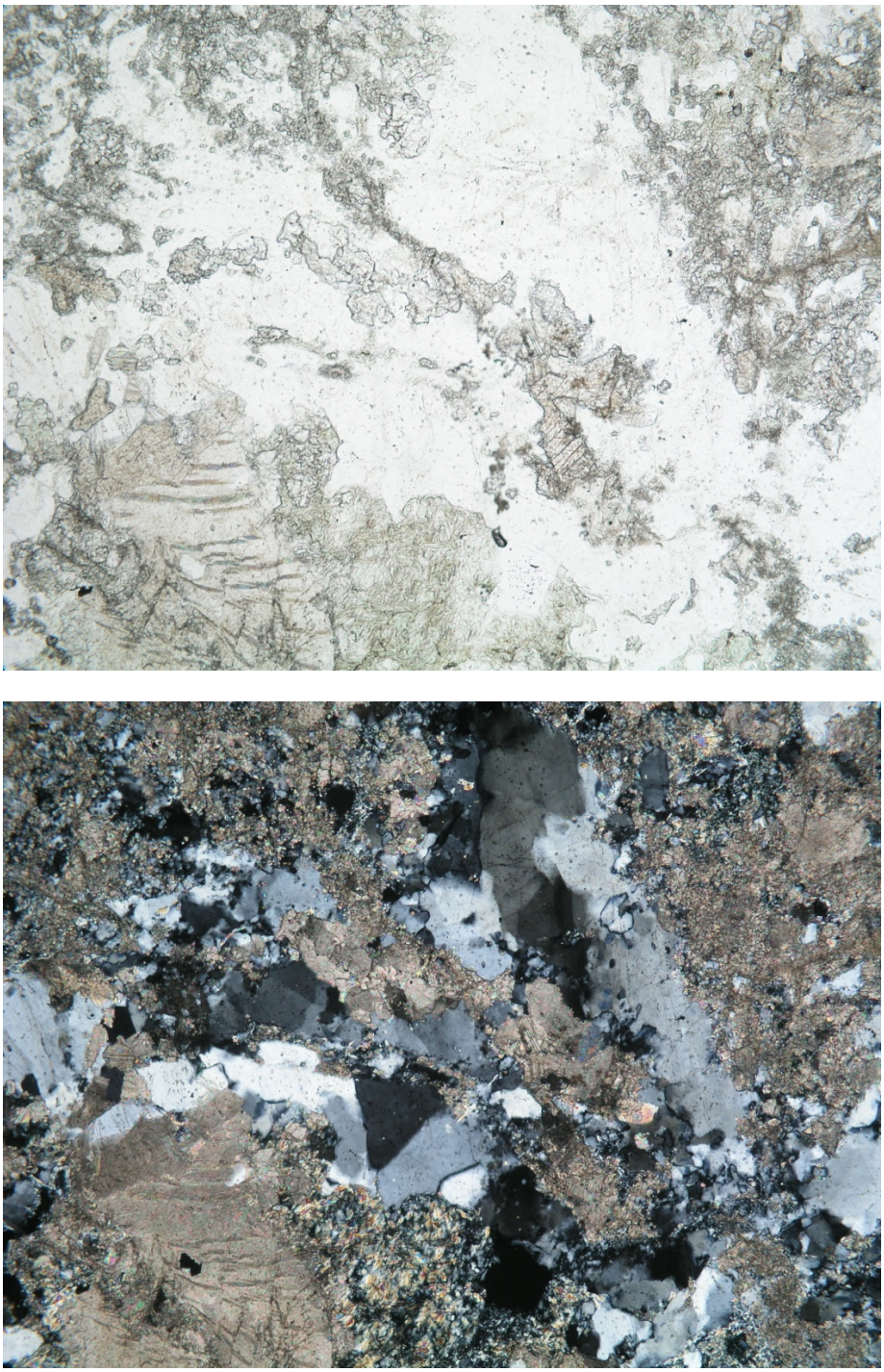

Fig. 3.23. Vein of quartz (colorless) and later calcite (colorless with high-relief). From 7490 ft in 83-11. Upper photomicrograph: plane polarized light; lower photomicrograph: crossed nicols. Field of view is 1.6 mm across.

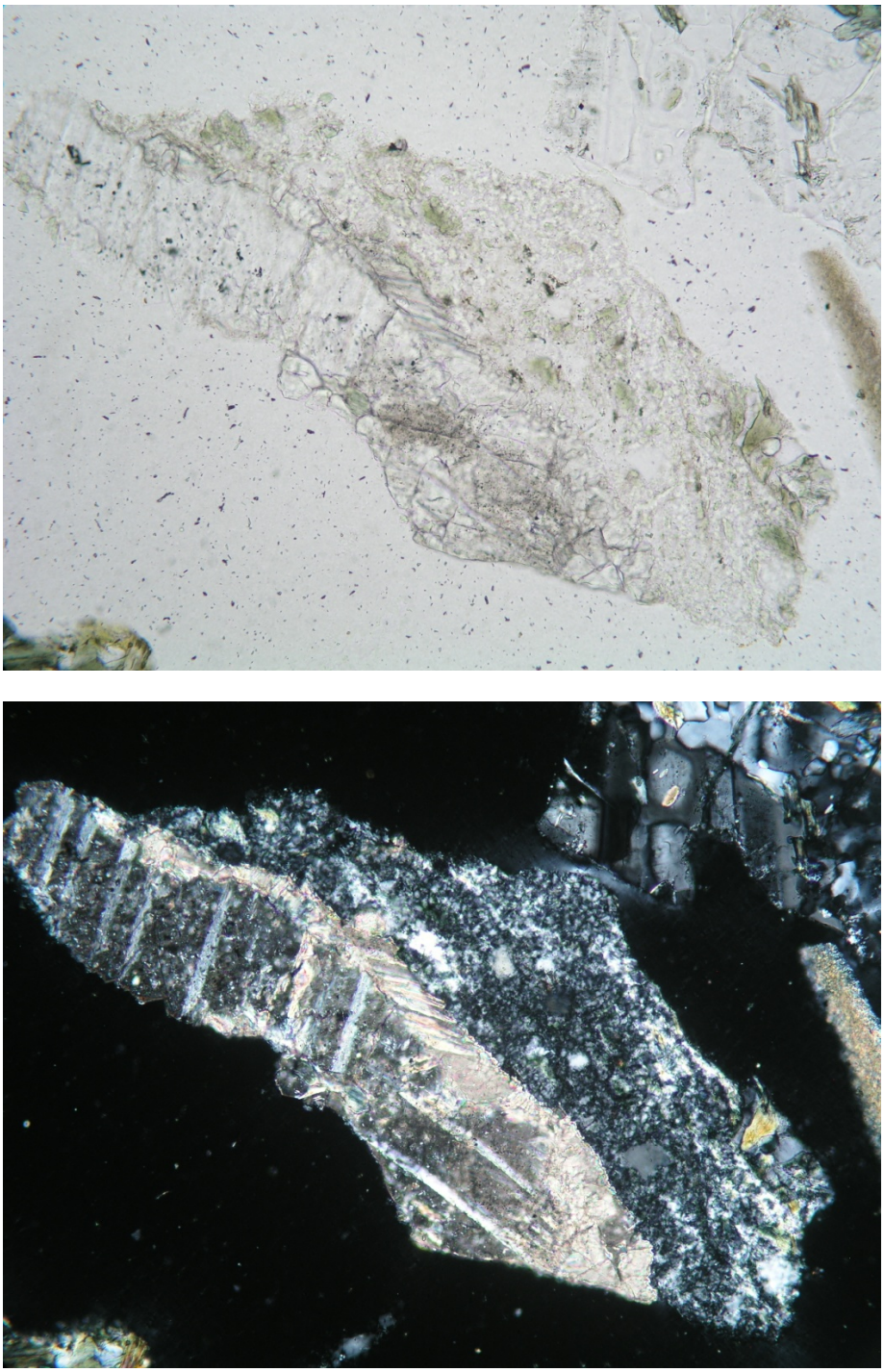

Fig. 3.24. Vein of calcite (left) cutting older brecciated quartz vein (right). The chip in the upper right is diorite. From 7260 ft in 83-11. Upper photomicrograph: plane polarized light; lower photomicrograph: crossed nicols. Field of view is 3.1 mm across.

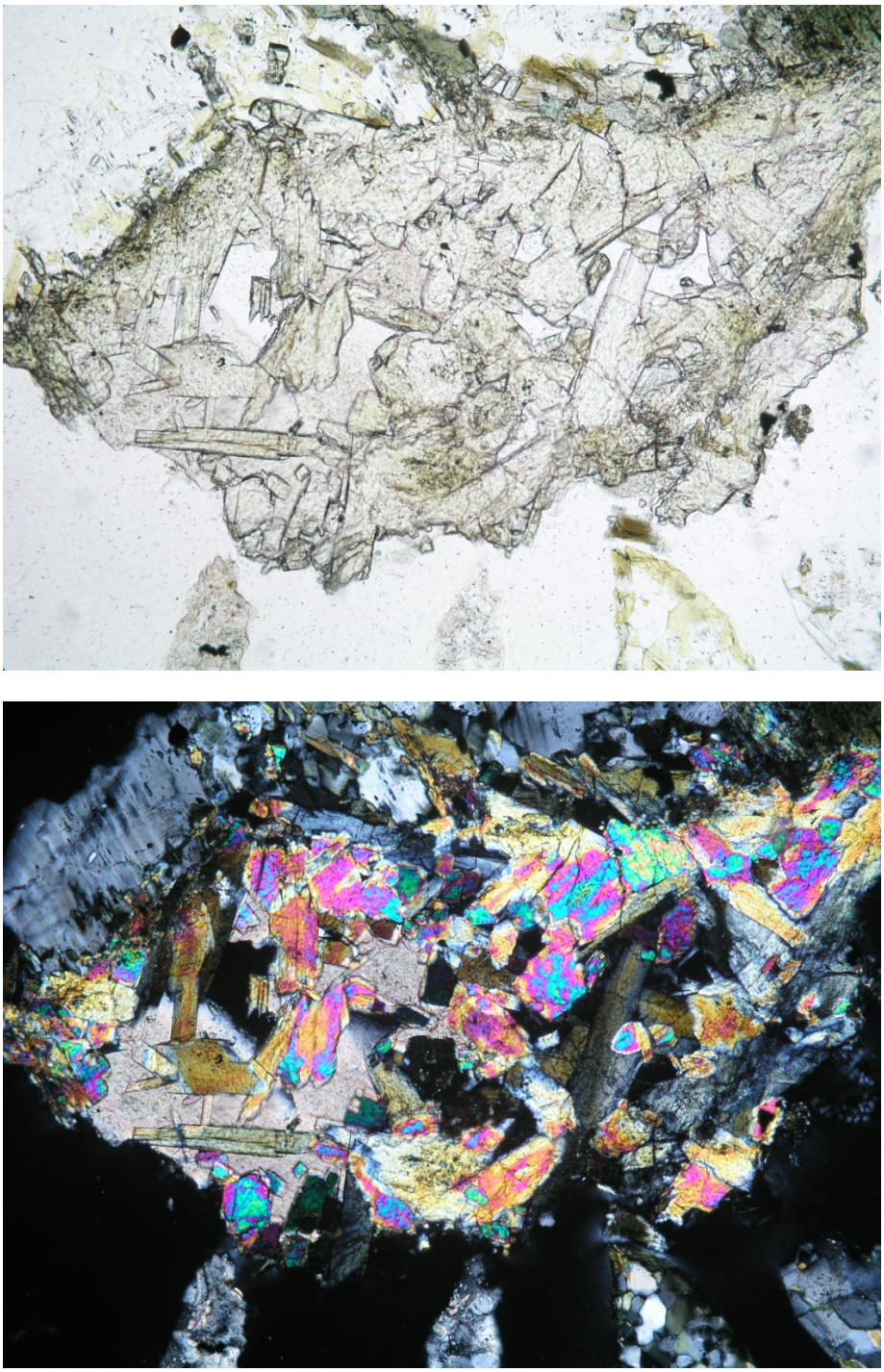

Fig. 3.25. Open epidote vein partially infilled with later calcite. Upper photomicrograph: plane polarized light; lower photomicrograph: crossed nicols. From 8080 ft in 33A-7. Field of view is 1.6 mm across.

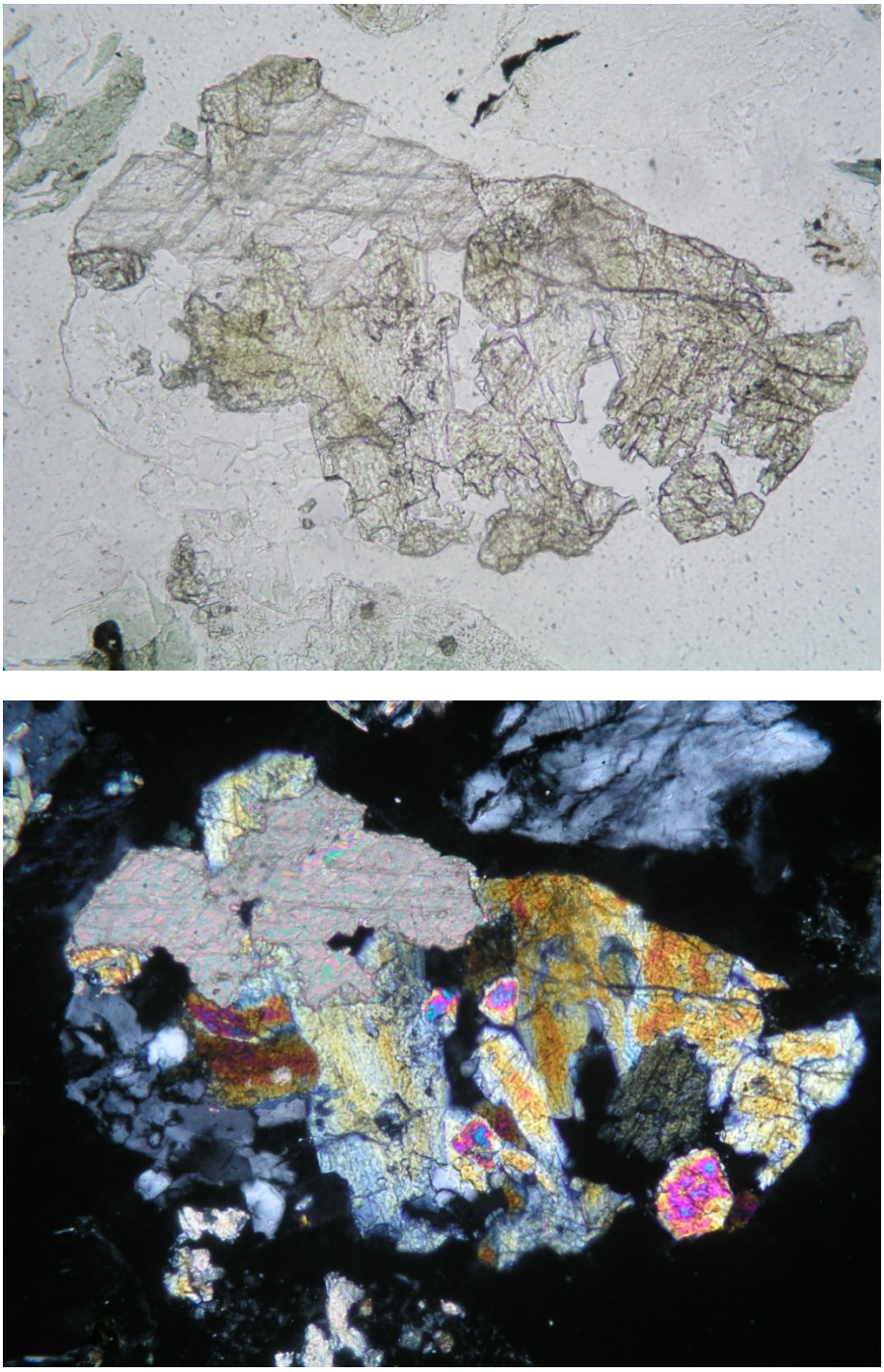

Fig. 3.26. Open vein ofadularia (not stained) epidote (colorless to yellow-green, high relief) and later calcite (colorless, two directions of cleavage visible). From 7370 ft in 33A-7. Upper photomicrograph: plane polarized light; lower photomicrograph: crossed nicols. Field of view is 3.1 mm across.

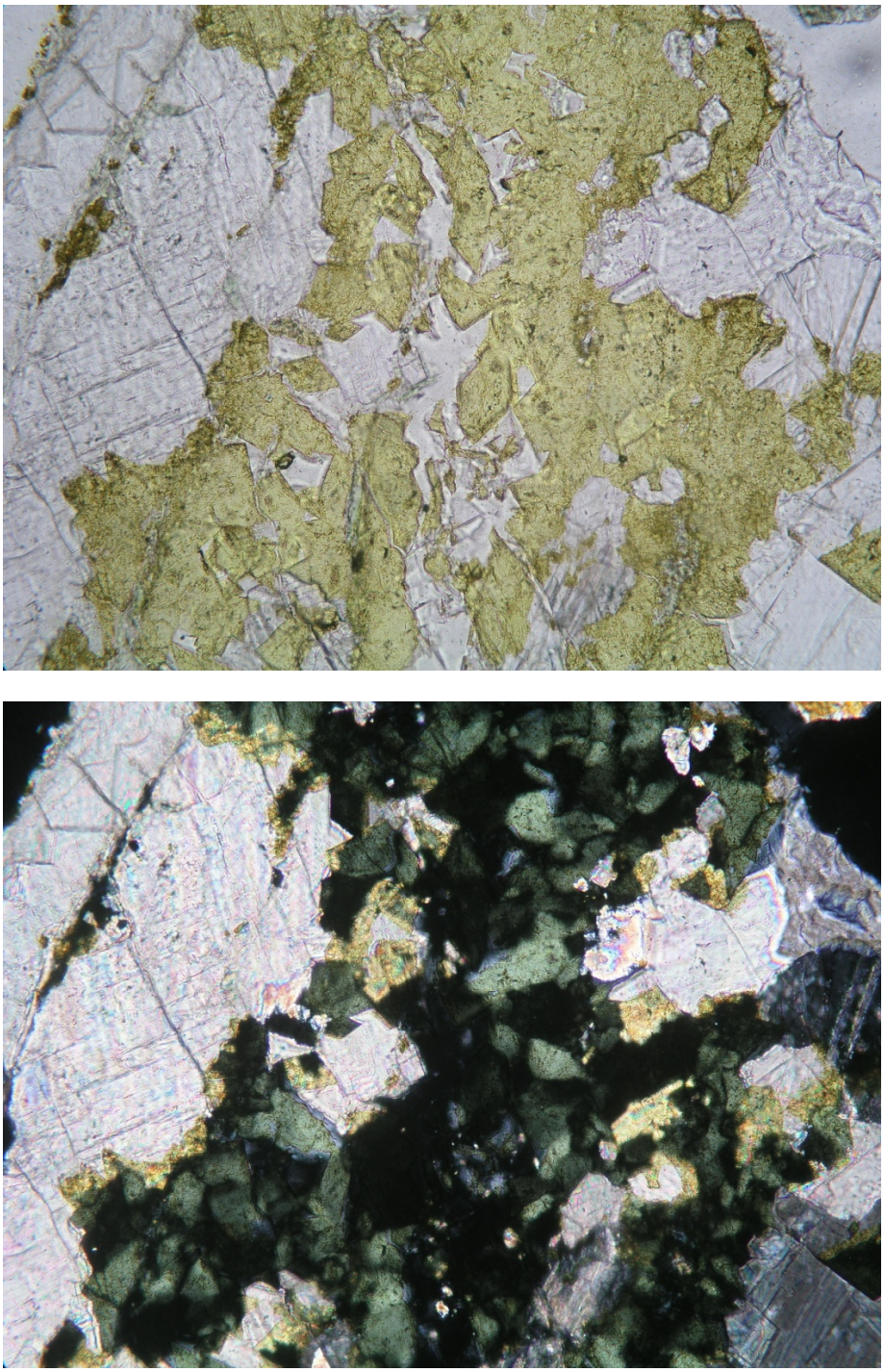

Fig. 3.27. Open vein containing early adularia (stained yellow) and later calcite. Upper photomicrograph: plane polarized light; lower photomicrograph: crossed nicols. From 6880 ft in 83-11. Field of view is 1.6 mm across.

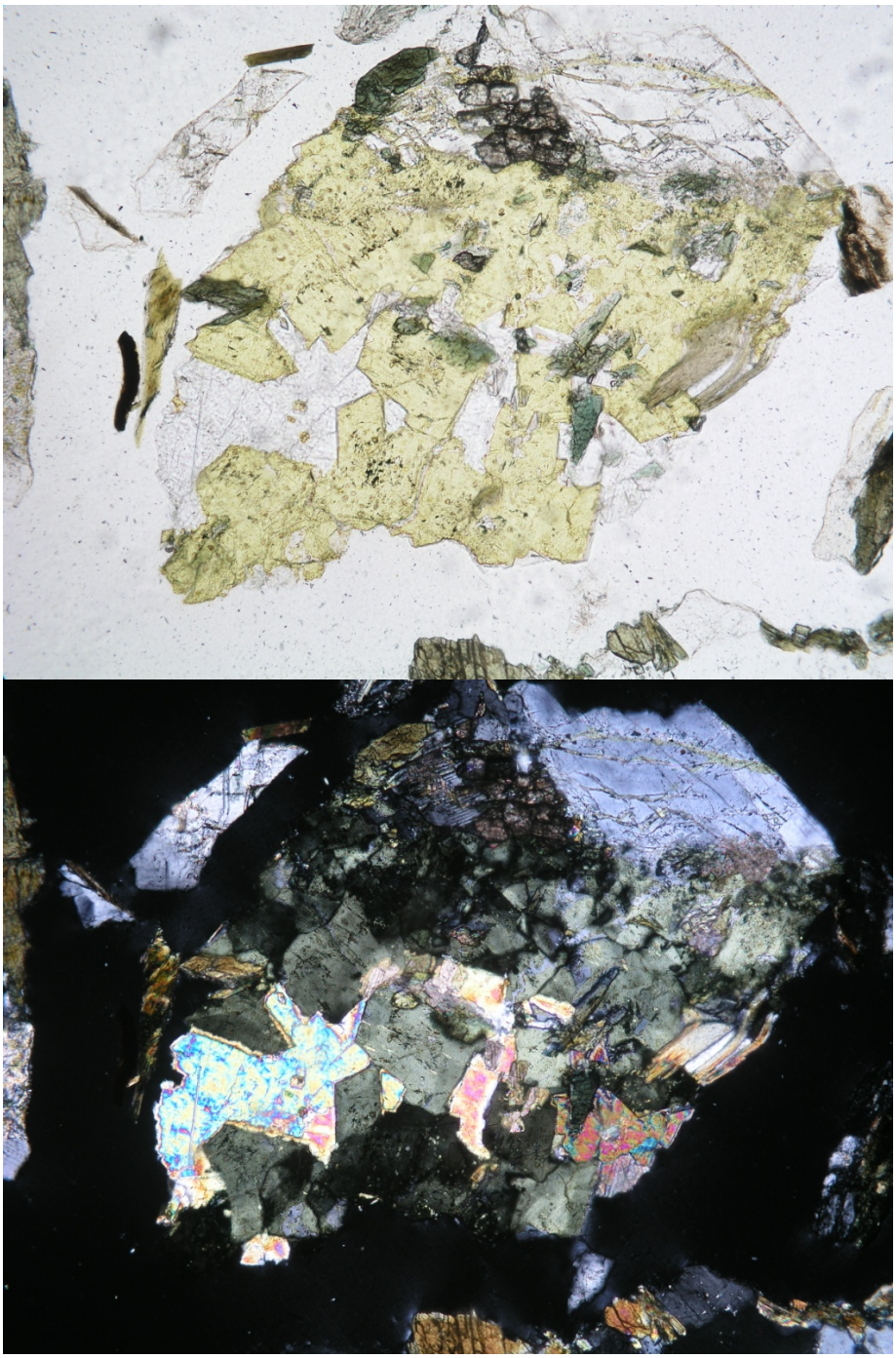

Fig. 3.28. Vein containing rhombic crystals of adularia (stained yellow) and later calcite in brecciated diorite. From 7250 ft in 83-11. Upper photomicrograph: plane polarized light; lower photomicrograph: crossed nicols. Field of view is 3.1 mm across.

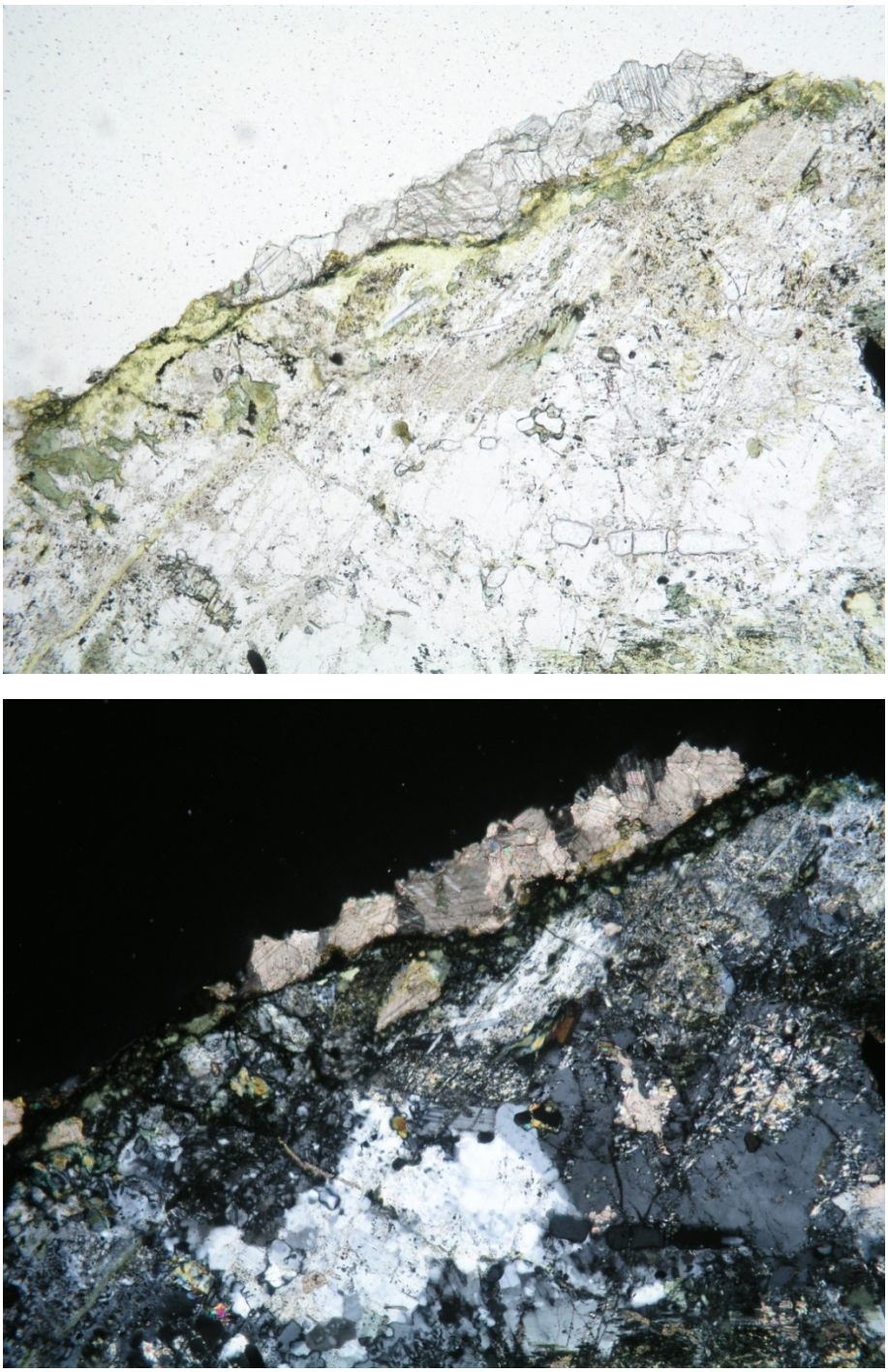

Fig. 3.29. Veins of early adularia (stained yellow) and later calcite cutting altered diorite. From 7340 ft in 33A-7. Upper photomicrograph: plane polarized light; lower photomicrograph: crossed nicols. Field of view is 3.1 mm across.

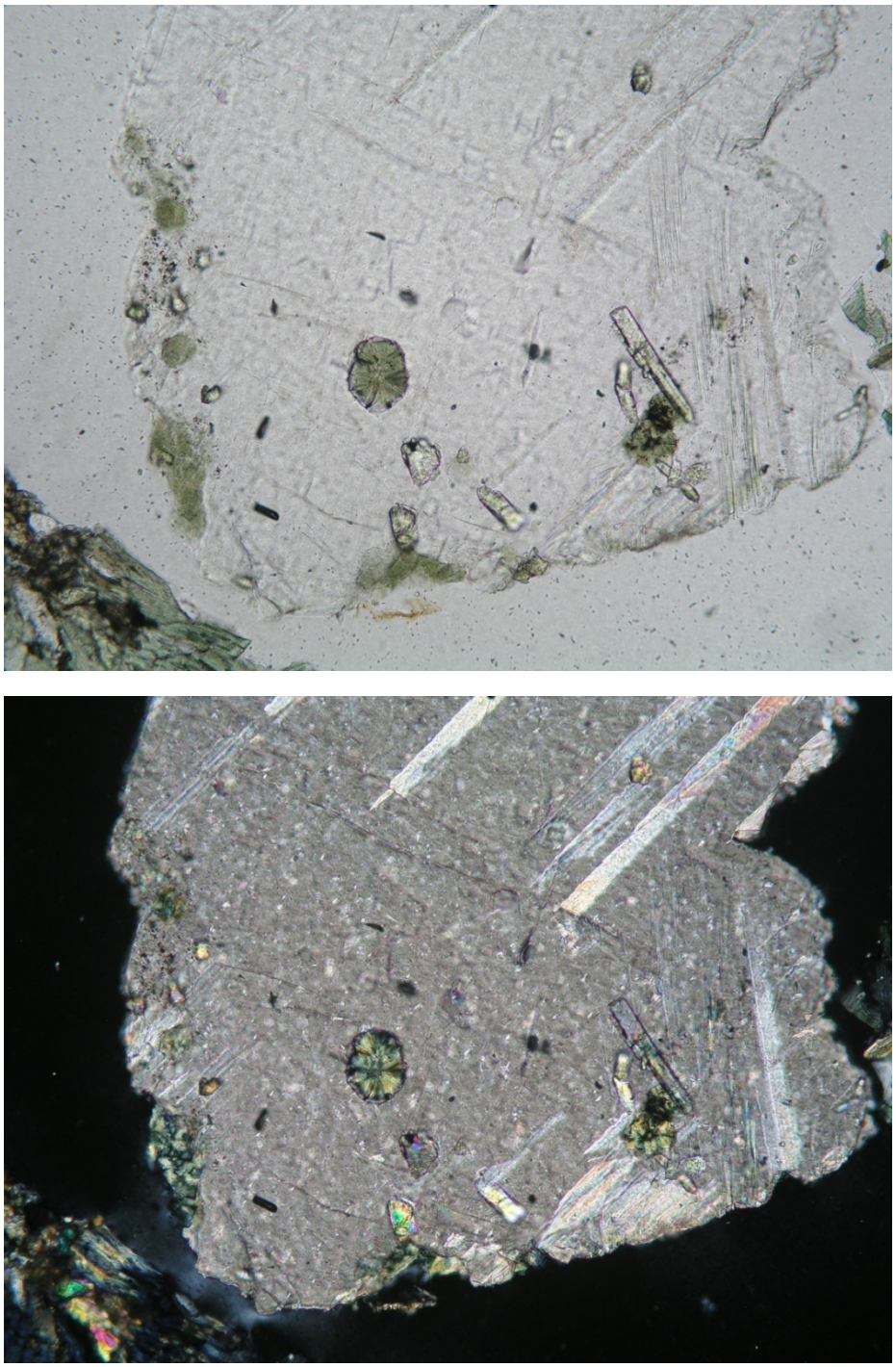

Fig. 3.30. Calcite that has encapsulated earlier chlorite (green) and prismatic epidote (colorless to yellow-green, high relief). From 7190 ft in 33A-7. Upper photomicrograph: plane polarized light; lower photomicrograph: crossed nicols. Field of view is 0.8 mm across.

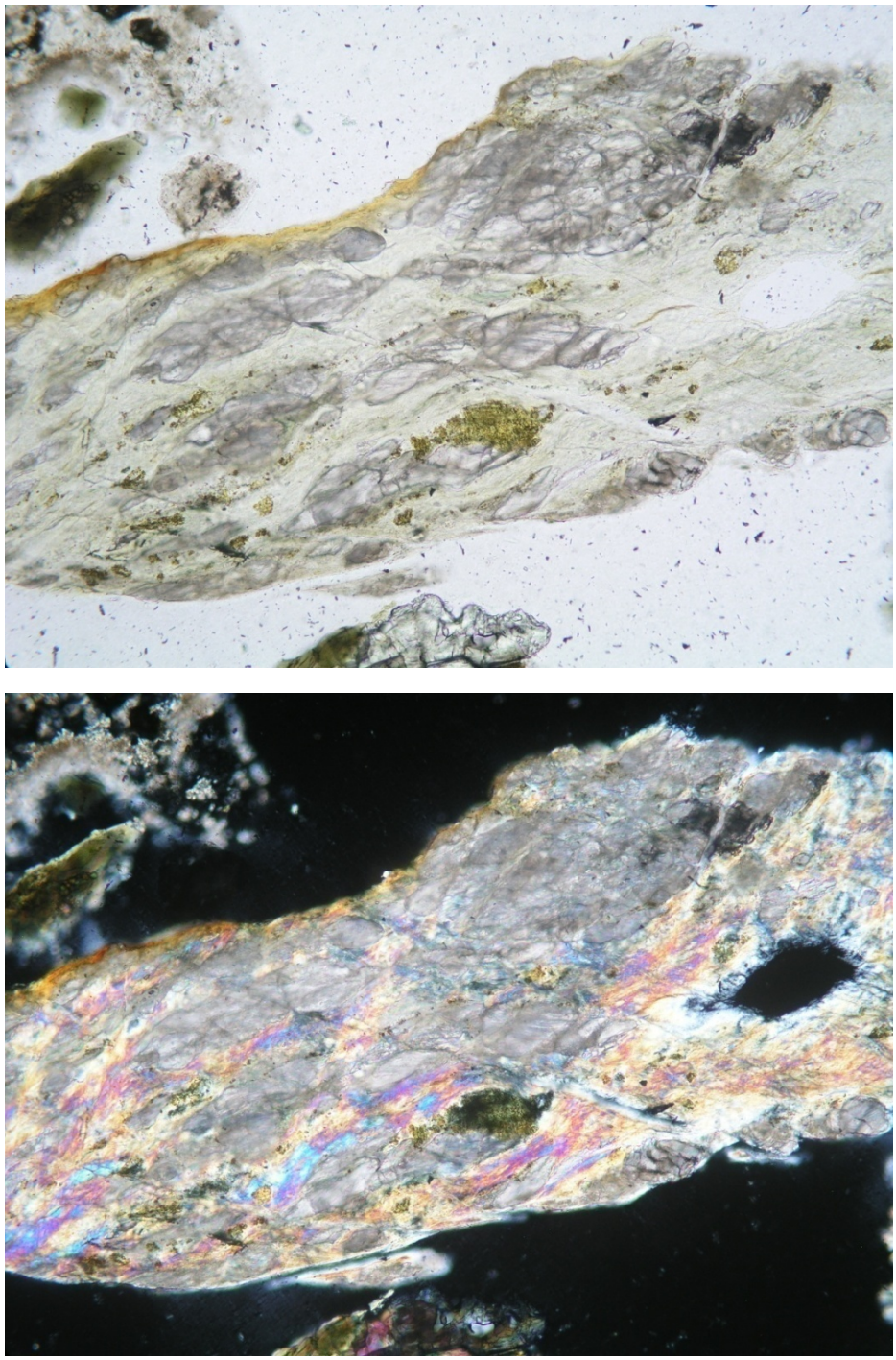

Fig. 3.31. Sheared vein consisting of calcite (moderate relief), illite and adularia(stained yellow). From 7040 ft in 33A-7. Upper photomicrograph: plane polarized light; lower photomicrograph: crossed nicols. Field of view is 3.1 mm across.

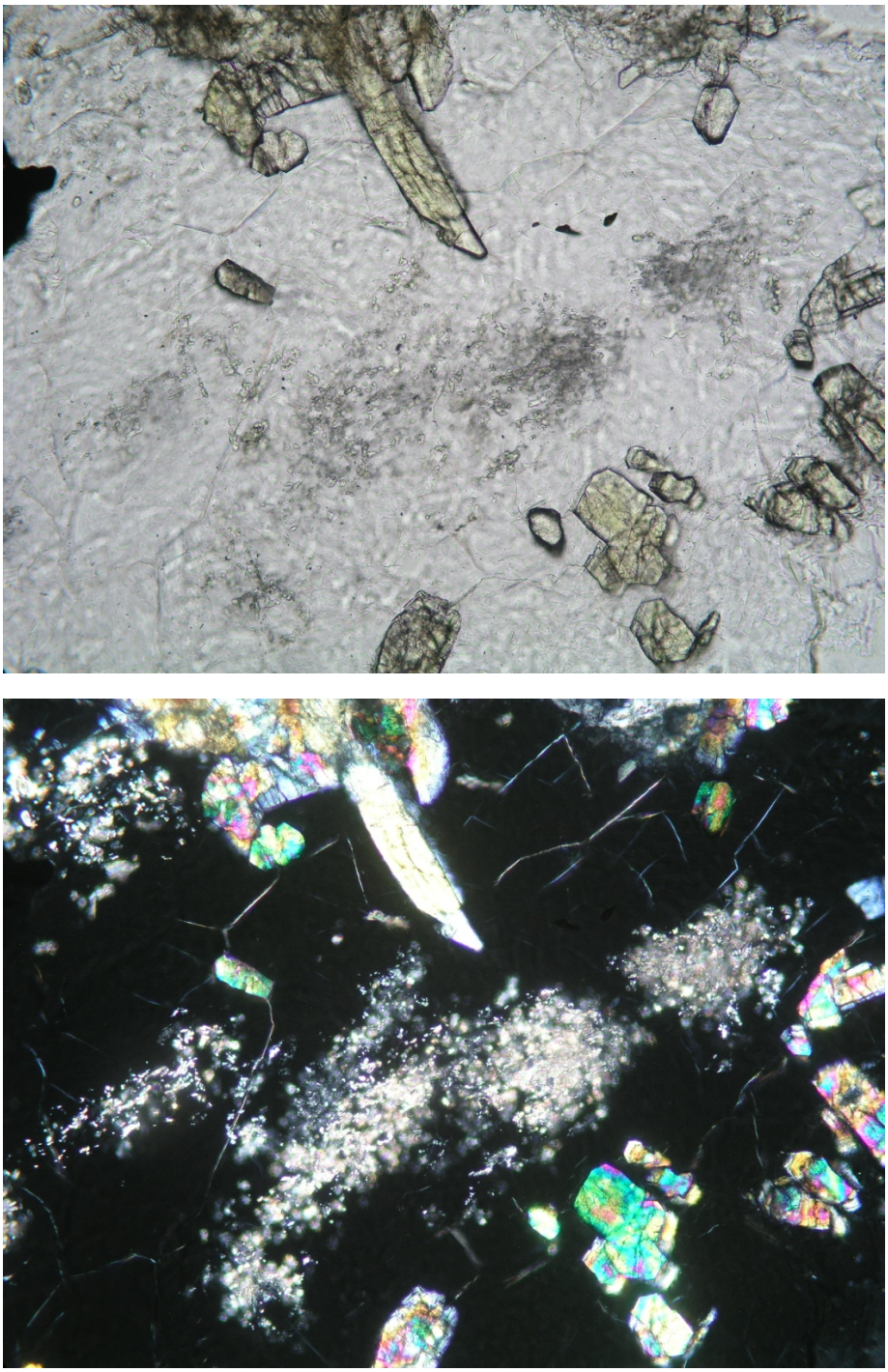

Fig. 3.32.Vein of fluorite (colorless) containing earlier epidote (colorless to yellow-green, high relief) and calcite (small high relief crystals in center of image). Upper photomicrograph: plane polarized light; lower photomicrograph: crossed nicols. From 9160 ft in 33A-7 ST-1. Field of view is 0.8 mm across.